ORIGINAL PAPER

Integrating facies, mineralogy, and paleomagnetism to constrain the age and provenance of Paleozoic siliciclastic sedimentary rocks along the northern Gondwana margin: insights from the Araba and Naqus formations in western Gulf of Suez, Egypt

Ashraf M. Al-Nashar[1] · Nabil A. Abdel Hafez[1] · Mohamed W. Abd El-Moghny[1] · Ahmed Awad[2] · Sherif Farouk[3] · Haitham M. Ayyad[1]

Abstract

The depositional ages and provenance of the Paleozoic Araba and Naqus Formations along the northern Gondwanan margin in Egypt have remained uncertain due to a lack of index fossils. Resolving this issue is crucial for understanding regional geology during deposition and subsequent tectonic development. We integrate detailed facies analysis, anisotropy of magnetic susceptibility (AMS), paleomagnetism, and mineralogical data to elucidate the genesis and depositional ages of the Araba and Naqus Formations. Petrographic analyses identified seven distinct facies types, providing insights into sedimentary textures, maturity, and sources, with contributions from igneous and metamorphic sources indicated by heavy minerals. X-ray diffraction (XRD) analysis identified accessory minerals such as quartz, goethite, kaolinite, hematite, and anatase. Paleomagnetism isolated two magnetic components (C_A and C_N) providing the first robust paleo pole positions at Lat. = 70.8° N, Long. = 308.2° E and Lat. = 37.8° N, Long. = 233.1° E, indicating Cambrian and Carboniferous ages for the Araba and Naqus formations, respectively. Thermal demagnetization constrained these dates using established polarity timescales. Mineralogical data indicated that the Araba Formation originated from an igneous source, while the Naqus Formation had a mixed metamorphic-igneous provenance. The integrated AMS and paleomagnetic data reveal evidence of post-depositional deformation. Specifically, the clustering of maximum AMS axes in the NW–SE direction for both formations, suggests the initial presence of a primary depositional fabric. However, prevalent tectonic activity during the Cenozoic appears to have overprinted and modified this fabric through deformation related to rifting of the Gulf of Suez region. Through this novel multi-proxy approach, we have resolved long-standing uncertainties regarding the formations' depositional ages. Our study thereby provides the first chronostratigraphic framework for these strategically important sedimentary units, significantly advancing understanding of regional Paleozoic geology.

✉ Haitham M. Ayyad
goldenayyad@azhar.edu.eg; goldenayyad@yahoo.com

1 Geology Department, Faculty of Science, Al-Azhar University, Nasr City, Cairo, Egypt

2 National Research Institute of Astronomy and Geophysics (NRIAG), Helwan, Cairo, Egypt

3 Exploration Department, Egyptian Petroleum Research Institute, Nasr City, Cairo, Egypt

Introduction

The history and evolution of Earth's ancient landmasses remain a subject of intense scientific inquiry. In particular, the vast supercontinent of Gondwana, which existed from the Late Precambrian to Jurassic periods, is a significant component of Earth's geologic narrative. Among the varied terrains that once constituted Gondwana, the Paleozoic siliciclastic sedimentary rocks spanning its northern fringe hold a particularly enigmatic position. From the Arabian Gulf in the east to Morocco in the west, this continuous

a 510 Ma Middle Cambrian
- Land
- Shallow Shelf
- Deep Shelf
- Ocean
- Evaporites
- Study Area

b LATE CARBONIFEROUS: 310 Ma
- Mid-ocean rift
- Subduction
- GONDWANA Supercontinent
- LAURUSSIA Supercontinent
- HUN Superterrane
- CIMMERIA Superterrane
- Other

- Studied succession
- Faults
- Subway
- Main Road
- Quaternary Deposits
- Miocene Deposits
- (M. Eocene) Mokattam Formation
- (E. Eocene) Thebes Formation
- Cretaceous Rocks
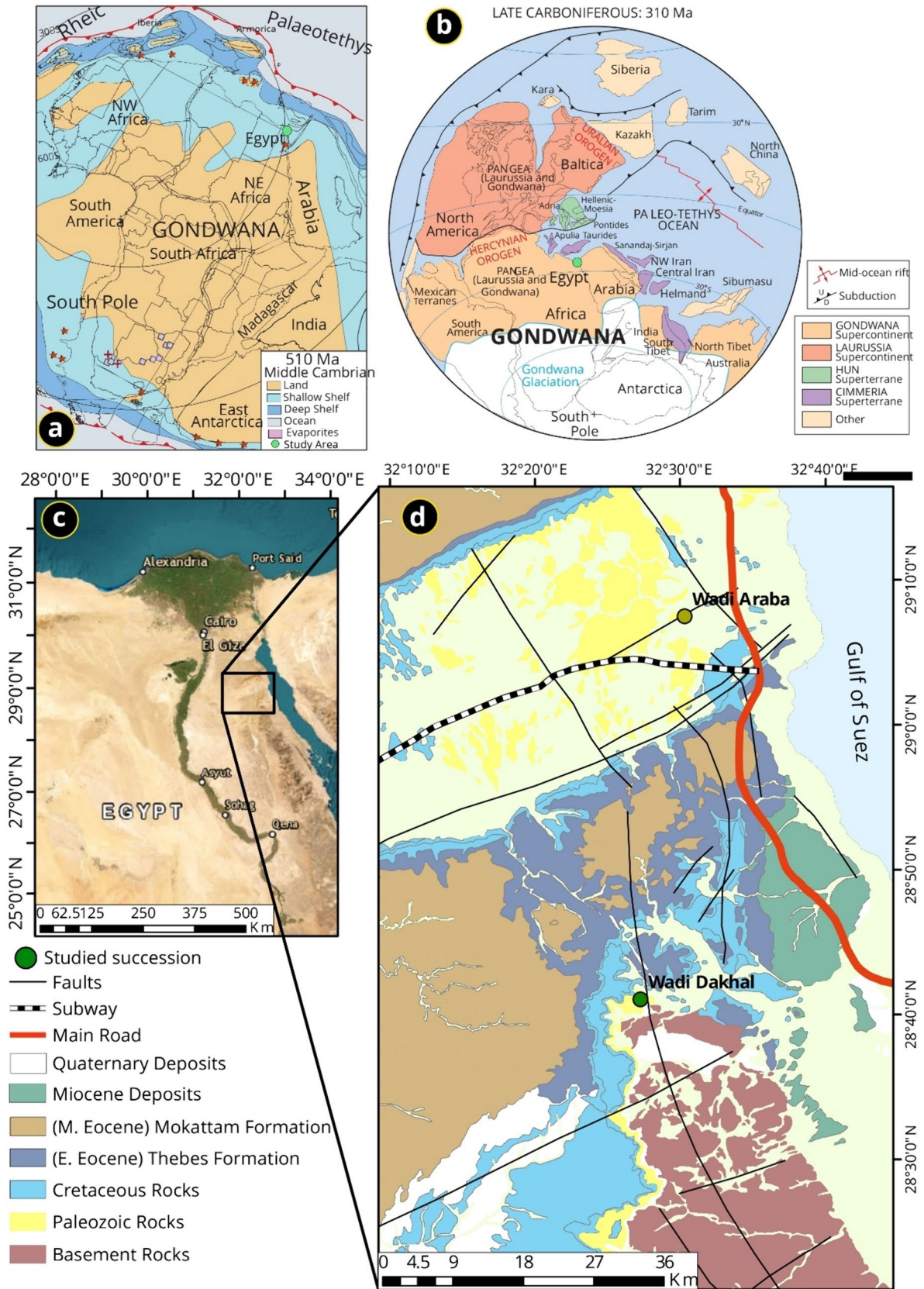- Paleozoic Rocks
- Basement Rocks

◄**Fig. 1** **a** Paleogeography of the central Gondwana area during the Middle Cambrian (510 Ma) according to Torsvik and Cocks (2011). **b** Plate tectonic global map of the late Carboniferous, showing the tectonic elements' positions at 310 Ma based on Torsvik and Cocks (2004). **c** Map indicating the research area's location in Wadi Dakhl, Egypt's Eastern Desert, along the northern margin of Gondwana, in the western Gulf of Suez. **d** Geological map illustrating the geographic placement of the studied section in Wadi Dakhl, situated along the northern margin of Gondwana in the western Gulf of Suez. It also displays the distribution of the investigated formations based on Conoco's (1987) findings

zone was part of what is now North Africa (Fig. 1a, b), characterized by a layering of shallow siliciclastic rocks (Murphy et al. 2004; Eschard et al. 2005; Ghienne et al. 2007a; Toto et al. 2008; Ghandour et al. 2013; Cambeses et al. 2017; Elhebiry et al. 2020; Omer et al. 2021; Şengör et al. 2022). However, unveiling the stories encrypted within these rocks, particularly concerning their provenance and age, is no straightforward task. The Paleozoic Era witnessed North Africa's role as an integral segment of Gondwana (Fig. 1a, b), post its assembly after the Pan-African orogeny (Powell et al. 1993; Burke and Lytwyn 1993; Meert and Van Der Voo 1997; Gürsu and Göncüoglu 2006; Ghienne et al. 2007b; Murphy et al. 2014; Ouabid et al. 2021; Gao et al. 2023). The sedimentary rocks from this epoch not only hold clues about past geodynamics but also have current implications, especially along the Gulf of Suez (Fig. 1c, d).

However, despite their importance, a cloud of ambiguity looms over the precise age of these sedimentary rocks, especially those lining the western peripheries of the Gulf of Suez (Chukhrov et al. 1966; Soliman and Abu El-Fetouh 1970; Razvalyayev 1972; Issawi and Jux 1982; Eames 1984; Nassr 1985; Klitzsch et al. 1990; Ibrahim 1996; Wanas and Soliman 2001; Wanas 2011; Hou et al. 2018; Abd-Elhameed et al. 2021; Said and Sakran 2022). Conventional stratigraphic techniques, such as studying fossils, offer limited insights due to the notable absence of diagnostic fossils in many formations. The Araba and Naqus formations, for instance, have been assigned a myriad of age brackets by various researchers, stemming from Early Cambrian to Carboniferous periods (Hassan 1967; Gvirtzman and Weissbrod 1984; Beleity et al. 1986; El-Shahat and Kora 1986; Allam 1989; Seilacher 1990; Abdallah et al. 1992; Schütz 1994; Salem et al. 1998; Abdeldayem 2003; Tawfik et al. 2012, 2015; Kozdrój et al. 2018). The challenge amplifies further due to the dearth of radiometric dating and bio-stratigraphically significant body fossils (Ghandour et al. 2013).

Amidst this backdrop, the current study emerges with a dual intent. First, it seeks to unravel the origin of these Paleozoic siliciclastic sedimentary rocks along the Gulf of Suez, harnessing clues from mineral inclusions and the morphological attributes of quartz. Second, it aims to redefine and refine the age determinations of the Araba and Naqus formations using palaeomagnetism, a promising tool that might break the existing stratigraphic impasse. Through an integrated application of microfacies analysis, this article aims to shed light on the provenance and age of these ancient deposits, providing a fresh perspective on the intricate geologic tapestry of the northern margins of Gondwana.

Geologic setting

The study area has a complex geological history from the Neoproterozoic to the present day. It is located in northeastern Africa and is part of the larger East African Orogen, which occurred when the Gondwana supercontinent amalgamated (Fig. 1a, b). During the Neoproterozoic, the closure of the Mozambique Ocean led to the collision of East and West Gondwana, resulting in the East African Orogeny. This orogenic event is divided into two main belts: the Mozambique Belt (MB) south and the Arabian-Nubian Shield (ANS) north. The ANS primarily consists of Neoproterozoic volcanic arcs, gneisses, metagabbros, metavolcano-sedimentary sequences, granites, and gabbro-diorite complexes (Stern 1985; Ali et al. 2010; Farahat et al. 2011; Abdelfadil et al. 2022; Sehsah and Eldosouky 2022; El-Bialy et al. 2023; Abd El-Wahed and Attia 2023). After the Neoproterozoic orogeny, the region experienced a period of relative tectonic stability during the Paleozoic era. Deposition began on the surface of the cratonic igneous and metamorphic basement, forming a distinct erosional unconformity. The main craton was formed during the Archean period, and subsequent tectonic processes, including the Pan-African Orogeny, further shaped the region and established major sedimentary basins during the Phanerozoic era. At the beginning of the Cambrian period, the study area, particularly Egypt, displayed a highly irregular shield area characterized by numerous ridges and depressions (Afanas'yev et al. 1965; Pickerill 1983; Abdel-Rahman and Martin 1987; Semtner and Klitzsch 1994; Khedr 2010; Fernández-Suárez et al. 2014; Andresen et al. 2014; Mohammad et al. 2020). The structural evolution in northeastern Africa, particularly in the study area, was likely influenced by regional extension

during the Pan-African orogenic phase, leading to the development of prominent ENE–WSW oriented planar fabrics in metamorphic rocks (O'Brien et al. 1983; Schandelmeier et al. 1988; Maurirv 1993; Tchameni et al. 2016; Mvondo et al. 2023). Foliation patterns defined by the preferred orientation of phyllosilicate minerals indicate extension directions during Pan-African orogenesis.

During the Paleozoic Era, epeirogenic movements led to various topographic highs, lows, and intracratonic basins, including the Northern Egypt basin and the Nile basin. The irregularity of the intracratonic basement paleorelief impacted the deposition of Paleozoic sedimentary rocks in Egypt, affecting their nature, type, distribution, thickness, and depositional conditions (Kruglyakov and Kruglyakova 1967; Issawi and Osman 1996). The thickness of these sedimentary rocks increases as one moves northward (Said 1990). Throughout the Early Paleozoic, North Africa experienced a series of tectonic activities, including tilting, fracturing, igneous intrusions, and transgression-regression cycles (Fabre 1988; Xu et al. 1997; Khedr 2010; Hammed et al. 2022). The studied Wadi Dakhl area is located in the northern Eastern Desert of Egypt, west of the Gulf of Suez (Fig. 1c, d). In this region, the Proterozoic basement is unconformably overlain by the siliciclastic Araba and Naqus formations, as well as a thick marine succession from the Late Cretaceous to the Eocene (Fig. 2a, b) (Issawi and Jux 1982; El-Barkooky 1986; Abdallah et al. 1992; Tawfik et al. 2011; Wanas 2011). The siliciclastic Paleozoic rocks in Wadi Dakhl consist of the Araba Formation at the base and the Naqus Formation above (Fig. 2a; Abdallah et al. 1992). These formations are exposed in limited areas along the Eastern Desert, such as north Wadi Qena, Wadi Dakhl (Fig. 1d), and Gabal El Zeit (Hassan 1967; Said 1990; Wanas and Soliman 2001; Khalifa et al. 2006; Wanas 2011).

The Araba Formation corresponds to Cambrian sandstone, which overlies the basement rocks in the Gabal Araba-Abu Durba region in southwest Sinai. It forms part of the Lower Paleozoic clastic sequence described by Hassan (1967). The thickness of the Araba Formation varies, ranging from 120 m at the type locality in the Gabal Araba–Abu Durba area (Seilacher 1990) to 25 m in the Eastern Desert (Issawi and Jux 1982) and up to 50–60 m thick in north Wadi Qena, Eastern Desert (Abdallah et al. 1992). In the studied area, the Araba Formation is characterized by alternating flat and lenticular beds of sandstone and mudstone. Towards the basal part, it transitions to cross-bedded coarse-grained to gravelly sandstone, with intercalations of shale, conglomerate, glauconitic sandstone, and very hard siltstone

(Fig. 2a). The conglomerates and pebbles directly overlie the Precambrian basement rock and form the basal part of the Araba Formation (Fig. 2c). The contact between these conglomerates and the basement rock is typically erosional and unconformable, indicating a significant time gap between their deposition.

The Naqus Formation, which overlies the Araba Formation, is predominantly composed of sandstone and mudstone with varying thicknesses. It ranges from a few meters in some areas to over 400 m in the southern Eastern Desert (Issawi and Jux 1982). The Naqus Formation in the Wadi Dakhl area is characterized by fine to medium-grained sandstone with interbedded mudstone and siltstone layers (Fig. 2d). The sandstone beds often exhibit cross-bedding and ripple marks, indicating deposition in a fluvial or tidal environment (Fig. 2e, g). The mudstone and siltstone layers are usually grey to black and may contain fossil remains, such as plant fragments and trace fossils. A notable feature of these sandstones is the presence of secondary structures, such as mashrabia or fenestra structures, which are formed by termite penetration and the borrowing of white sand. The mashrabia structures are primarily found in the basal part of the succession (Fig. 2d), while complex jointing is more common, especially in the uppermost part of the succession (Fig. 2f).

Considering the broader geologic context, the study area in northeastern Africa has undergone a complex history of tectonic events, including the Neoproterozoic East African Orogeny and the subsequent Pan-African Orogeny. These events have influenced the deposition of sedimentary rocks from the Paleozoic to the present day, resulting in a diverse array of rock types and structural features. The geology of Wadi Dakhl offers valuable insights into the tectonic and sedimentary processes that shaped ancient Egypt and the broader Paleozoic dynamics of the northern Gondwana margin. A comprehensive characterization of the Araba and Naqus formations would greatly benefit economic endeavors and tectonic reconstructions.

Material and methods

Fieldwork was conducted to measure and sample two stratigraphic formations, the Araba Formation and Naqus Formation, exposed along the western edge of the Gulf of Suez in Wadi Dakhl (Fig. 1c, d). Measurements and sampling were carried out within the Wadi Dakhl area spanning latitudes 28° 36′ 29″ to 28° 41′ 32″ N and longitudes 32° 20′ 6″ to

Fig. 2 **a** A columnar stratigraphic section of the investigated successions in Wadi Dakhl. The figure includes field photographs showcasing the distinctive field characteristics of the Araba and Naqus formations, as follows: **b** the photograph captures high relief basement rocks and highlights the boundary separating the Araba and Naqus formations. **c** The image illustrates conglomerates and pebbles found in the lower section of the Araba Formation. **d** The image displays complex jointing with planar cross-bedding in the upper part of the Naqus Formation. **e** A photograph showcases the ferruginous mudstone characteristic of the Naqus Formation. **f** A photograph exhibits trough cross-bedded sandstone or festoon cross-bedding observed in the Naqus Formation. **g** The photograph highlights the presence of the Mashrabia structure (also known as Fenestra structure), which is a distinctive feature found in the sandstones of the Naqus Formation

32° 28′ 23″ E (Fig. 1d). A total of 101 representative fresh block samples were collected from across the stratigraphic succession, including sandstone and mudstone lithologies. Additionally, 76 standardized oriented core samples were obtained from nine different localities, comprising 36 cores from the Araba Formation and 40 cores from the overlying Naqus Formation. All core samples consisted of unweathered and untilted sandstone. A portable rock drill machine equipped with a magnetic compass aided the collection of samples across the field area of Wadi Dakhl.

Petrographic analysis was performed to determine the provenance of sedimentary rocks. Fourteen thin sections of the sandstone samples were examined using a polarizing microscope to identify the mineral composition, texture aspects, and diagenetic features. The modal content of the sandstones was determined by counting 500 points per thin section. Granulometric characteristics such as grain size, sorting, and roundness were calculated by measuring the maximum diameter of 100 random grains per thin section under the microscope.

X-ray diffraction (XRD) analysis was conducted on four bulk mudstone samples and selected sandstone samples to identify their mineralogical composition. The analysis was performed using wavelength-dispersive X-ray fluorescence Spectrometry with a Philips-type Pan-Alytica X-pert-pro automated powder diffractometer system. The samples were analyzed using Cu-radiation ($\lambda = 1.542$ A°) at 40 kV and 30 mA, with an average scanning speed of 0.02°/S.
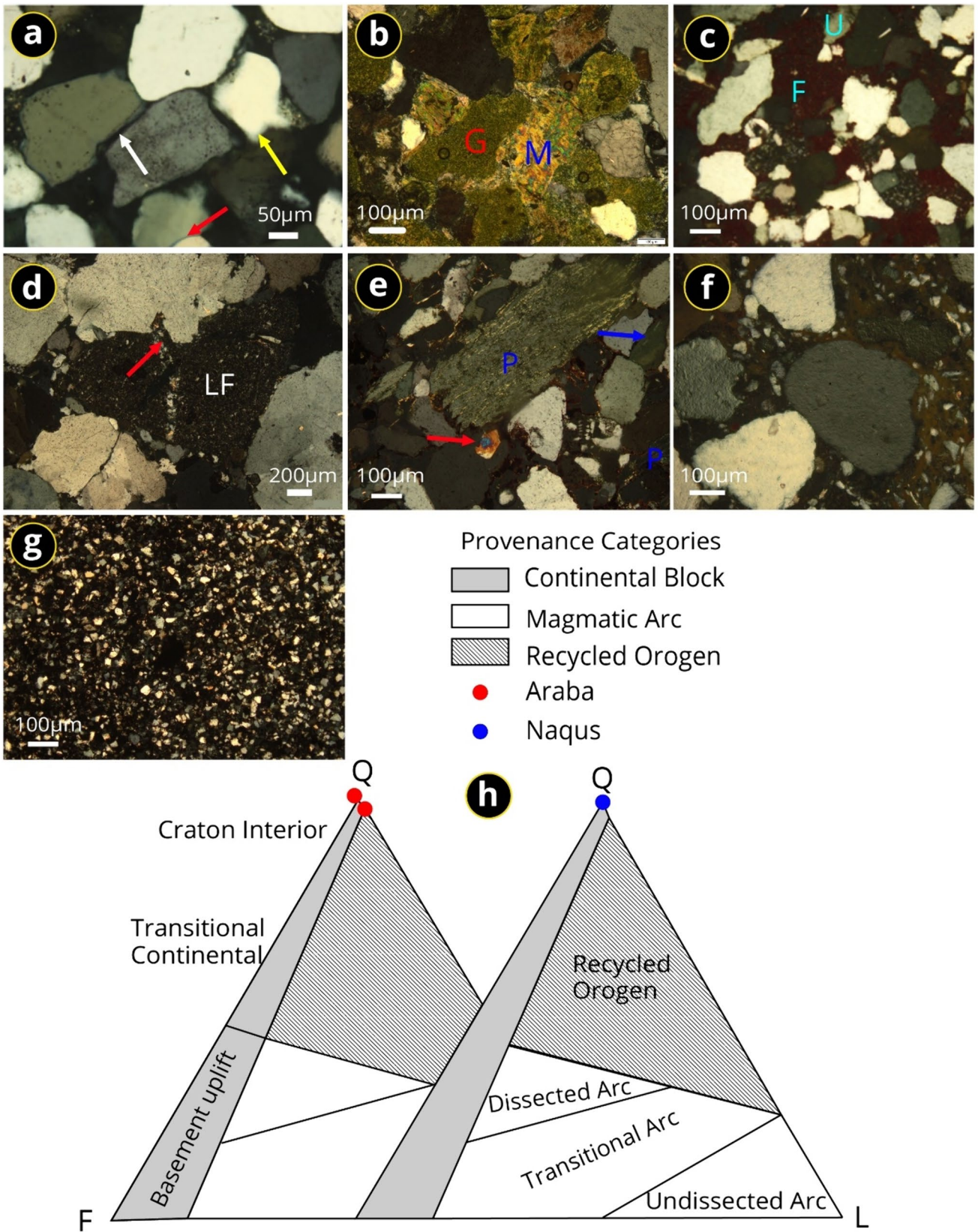
◄**Fig. 3** Photomicrographs of the examined sandstone samples, highlighting the presence of diverse microfacies types. **a** The photomicrograph displays a quartz arenite facies type (Naqus Formation, S.No. N3) under crossed-polarized light (XPL). It exhibits silica overgrowth (indicated by the white arrow), quartz grains with sutured contact (yellow arrow), and occasionally concave–convex grains (red arrow). **b** The image illustrates a glauconitic quartz arenite sandstone type (Araba Formation, S.No. A6) under XPL. It primarily consists of quartz and mica (M) and contains rounded glauconite pellets (G). **c** A photomicrograph showcases a ferruginous quartz arenite (Araba Formation, S.No. A10) under XPL. Some quartz grains exhibit undulose extinction (U), and all grains are cemented by iron oxide (F). **d** The image represents a sublith-arenite facies type (Araba Formation, S.No. A3), mainly composed of monocrystalline grains and lithic fragments (Lf) of claystone, observed under XPL. **e** A photomicrograph displays quartz sub-greywacke microfacies (Araba Formation, S.No. A2) under XPL. It consists primarily of monocrystalline grains and partially altered plagioclase (P), with zonation of zircon (z). **f** The image highlights a quartz greywacke facies type (Araba Formation, S.No. A9) under XPL, exhibiting scattered matrix. **g** The photomicrograph represents a ferruginous siltstone facies type (Araba Formation, S.No. A8) under XPL. **h** The figure includes QFL ternary provenance discrimination diagrams for the studied sandstones of the Araba and Naqus formations (Dickinson and Suczek 1979; Dickinson 1988)

The XRD analysis was carried out in the laboratory of the National Research Center in Cairo. Heavy mineral analysis was performed on seven unconsolidated sandstone samples. The sand samples were sieved and separated into grain size fractions, with the size fraction (0.500–0.125 mm) selected for analysis using gravity settling by bromoform (specific gravity 2.88). The separated heavy minerals were identified using binocular and scanning electron microscopes.

Paleomagnetic analysis was conducted on 78 oriented core samples collected from 6 sites within the Araba and Naqus formations. Specifically, 40 cores were obtained from 3 sites in the Araba Formation and 38 cores from 3 sites in the overlying Naqus Formation. The core samples were cut into 2.2 cm pieces at the National Research Institute of Astronomy and Geophysics (NRIAG) Rock Magnetism Laboratory in Helwan, Egypt for magnetic analysis. Extensive rock magnetic experiments were performed prior to paleomagnetic measurements, including stepwise isothermal remanent magnetization (IRM) acquisition and backfield curves up to 5T using an MMPM 10 pulse magnetizer attached to an AGICO JR6-A spinner magnetometer. Curie temperature determinations were made using a Kappabridge MFK1-FA instrument equipped with CS-L and CS4 units to measure low- and high-temperature variations in magnetic susceptibility. The Kappabridge system also measured anisotropy of magnetic susceptibility (AMS) to elucidate the

magnetic fabric of the rocks. AMS is based on the relationship between induced magnetization (*M*) and applied magnetic field (*H*), where $M = kHz$, and reflects the preferred orientation of magnetic minerals (Tarling and Hrouda 1993).

Paleomagnetic component isolation was achieved by thermally demagnetizing 76 representatives samples from each formation in ten steps from ambient temperature to 700 °C using an MMTD80 thermal demagnetizer. Natural remanent magnetization (NRM) and magnetic susceptibility were measured before and after each heating step using a Bartington MS3-system to monitor changes in magnetic minerals. This was performed in the NRIAG Rock Magnetism Laboratory using state-of-the-art equipment to analyze the magnetic properties and accurately isolate the paleomagnetic signal. This basic analysis of paleomagnetic data is usually obtained through alternating-field or thermal demagnetization procedures, using Remasoft 3.0 software. By integrating fieldwork with petrographic analysis, X-ray diffractometry (XRD), heavy mineral studies, AMS and paleomagnetic observations, we can establish a comprehensive understanding of the provenance and age of the Paleozoic sedimentary rocks along the northern Gondwana margin in the western side of the Gulf of Suez.

Results

Petrographic analysis

The clastic sedimentary rocks were classified based on the classification system proposed by Folk (1980). The petrographic examination of the studied sandstones and siltstones identified seven distinct facies types: quartz arenite, glauconitic quartz arenite, ferruginous quartz arenite, sublith-arenite, quartz sub-greywacke, quartz greywacke, and ferruginous siltstone.

Quartz arenite

The quartz arenite facies are predominantly observed in the Naqus Formation (Samples N1, N2, N3, N4, and N8). The framework of this facies consists of quartz grains comprising up to 99.3% of the rock composition, with occasional feldspars and rock fragments. The quartz grains are primarily mono- and polycrystalline, very fine to fine sand-sized, and exhibit subrounded to rounded shapes. The grains are mainly elongated, with minor occurrences of spherical grains, and are closely packed. Contact between quartz grains is

observed as point, concave–convex, and suture contacts. The high relative content of quartz grains compared to feldspar and rock fragments indicates a mature sandstone with a high degree of sorting. The grains are cemented by crystalline silica, and some pore spaces contain traces of authigenic kaolinite. Silica overgrowth is also observed, indicating diagenetic dissolution of the outer surface of certain quartz grains (Fig. 3a).

Glauconitic quartz arenite

This facies is found in the middle part of the Araba Formation (Sample A6). The framework grains primarily comprise quartz, with minor accessory minerals such as mica. The quartz grains are very fine sand-sized, sub-angular, and exhibit low sphericity. A few rounded glauconitic pellets (less than 4%) are also observed in this sandstone type (Fig. 3b). The occurrence of glauconite in the glauconitic quartz arenite facies suggests that the sediment was deposited in a marine setting with relatively low energy. Glauconitic pellets indicate the presence of organic material that underwent decay, releasing iron and potassium ions into the surrounding pore waters (Donald and Schwab 1996). These ions were then incorporated into the growing glauconite crystals.

Ferruginous quartz arenite

This sandstone type is well represented in both the upper parts of the Araba and Naqus formations (Samples A10 and N7). The framework primarily comprises quartz (> 99%) with trace amounts of mica flakes. The quartz grains are monocrystalline, moderately sorted, very fine to fine sand-sized, and exhibit sub-angular to subrounded shapes with low sphericity. Some monocrystalline quartz grains exhibit undulatory solid extinction. The grains are closely packed, showing point, concave–convex, and regular contacts. Iron oxide has cemented the sediment (Fig. 3c), indicating that iron minerals have been mobilized and precipitated under diagenetic conditions (Wang et al. 2019; Dreher et al. 2021).

Sublith-arenite

This facies are well developed in the lower part of the Araba Formation (Sample A3). It consists of quartz (monocrystalline and rarely polycrystalline), feldspar, and sedimentary lithic fragments. The modal composition of the sandstone is approximately 91.24% quartz, 3.5% feldspar, and 5.26% sedimentary lithic fragments. The quartz grains are moderately sorted, sub-angular, and subspherical and range from medium to coarse sand size, exhibiting a closely packed texture. Sedimentary lithic fragments, particularly claystone, are more common than feldspar. The feldspars in this facies include microcline and plagioclase grains (Fig. 3d).

Quartz sub-greywacke

These microfacies are observed in Araba and Naqus formations (Samples A2 and N6). The quartz sub-greywacke facies consist of fine sand-sized quartz grains that are subangular to subrounded in shape. The grains are primarily monocrystalline and occasionally polycrystalline. Some zircon grains may also be present in these facies. These facies exhibit a closely packed texture like the quartz arenite facies. The contact between grains is observed as point, concave–convex, and straight contacts. The matrix contains authigenic kaolinite, which formed because of feldspar alteration (Fig. 3e). The occurrence of authigenic kaolinite within the matrix of the quartz sub-greywacke facies suggests that feldspars underwent alteration due to diagenetic fluids.

Quartz greywacke

This sandstone type is well-developed at several intervals in the middle and upper parts of the Araba Formation (Samples A7 and A9). It comprises monocrystalline and rarely polycrystalline quartz grains ranging from very fine sand to coarse sand. The grains must be better sorted, subangular to subrounded, subspherical, and submature, exhibiting an open packing texture. The matrix comprises fine silty detrital grains and authigenic kaolinite (Fig. 3f).

Ferruginous siltstone

The ferruginous siltstone lithofacies are predominantly found in the middle parts of the Araba Formation (Sample A8). These facies consist of very fine sand, silty-sized, angular, and moderately sorted quartz grains. The grains are embedded in a clay matrix and cemented by iron oxide, giving them a reddish-brown color (Fig. 3g). Iron can be sourced from various minerals present in the sedimentary rocks, such as feldspars or iron-bearing clay minerals. Iron oxide in the matrix suggests diagenetic precipitation of iron minerals.

The framework minerals consist primarily of quartz, with varying amounts of feldspar, mica, and sedimentary lithic
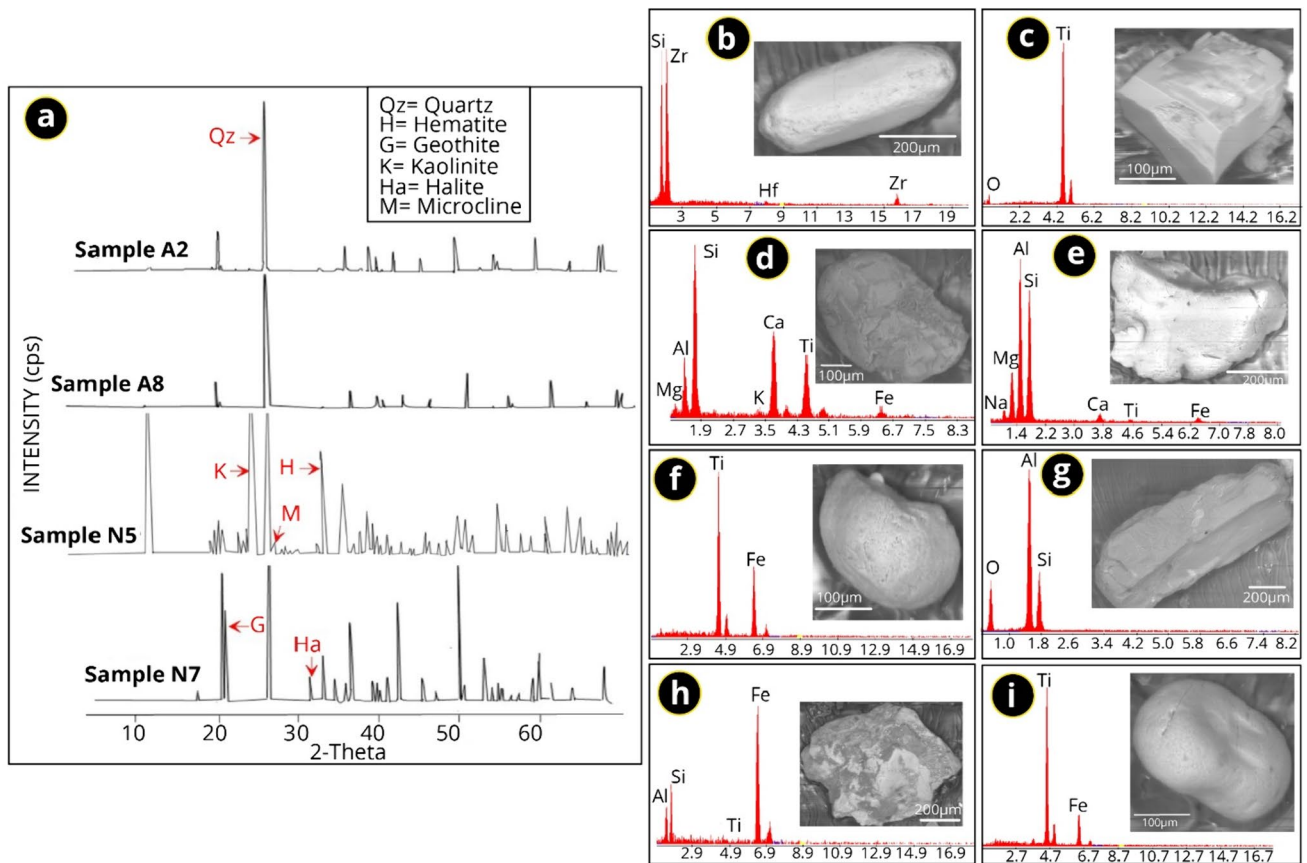
Fig. 4 A combination of XRD analysis and SEM images to provide a comprehensive understanding of the sandstone samples' mineralogical composition and the specific heavy minerals present within the studied sedimentary rocks. The figure includes the following components: **a** X-ray diffraction (XRD) patterns of select sandstone samples from both the Araba (A) and Naqus (N) formations. **b** An SEM image showcasing the identified heavy mineral zircon. **c** An SEM image displaying the identified heavy mineral rutile. **d** An SEM image showcasing the identified heavy mineral sphene. **e** An SEM image displaying the identified heavy mineral pyroxene. **f** An SEM image showcasing the identified heavy mineral ilmenite. **g** An SEM image displaying the identified heavy mineral andalusite. **h** An SEM image showcasing the identified heavy mineral magnetite. **i** An SEM image displaying the identified heavy mineral leucoxene

fragments (Fig. 3h). The grains' texture, sorting, rounding, and packing differ among the different facies' types. The presence of authigenic minerals such as kaolinite and iron oxide indicate diagenetic processes. The petrographic characteristics provide valuable insights into the depositional environments and diagenetic history of the studied sedimentary rocks.

X-ray diffractometry (XRD) analysis

XRD analysis was carried out on selected sandstone samples from the Araba and Naqus formations to identify their mineralogical composition (Fig. 4a). The primary mineral identified in all samples was quartz, the principal sandstone constituent. Goethite was also ubiquitous and likely formed as an alteration product of ferromagnesian minerals. Kaolinite was another common mineral detected, indicating the weathering of feldspars under acidic soil conditions. Hematite was present in minor amounts in some samples. Notably, calcite was exclusively found in samples from the Araba Formation, suggesting a transitional marine influence during deposition.

The Naqus Formation samples yielded additional essential results. Anatase (TiO_2) was identified as an accessory mineral averaging 2.3% concentration (Fig. 4a). This indicates derivation from bare igneous rocks within the source terrain (Hanaor and Sorrell 2011; Bowles 2021; Miah 2021). Microcline and halite were also detected exclusively in

Naqus sandstones. Microcline suggests the presence of an additional igneous source component since it is commonly found alongside other feldspar minerals, such as plagioclase grains (Haldar and Tišljar 2014). On the other hand, the polycrystalline quartz grains found in the Naqus Formation exhibit a mixture of straight and curved sutures, along with multiple extinctions. These characteristics strongly suggest that the majority of these polycrystalline quartz grains originate from the surrounding metamorphic rocks (Folk 1980). Meanwhile, halite supports evaporitic conditions during the deposition of upper Naqus sedimentary rocks.

Overall, the XRD data are consistent with petrographic observations of a dominant quartz arenite composition. However, accessory minerals provide insight into subtle provenance variations between the formations. Consequently, the XRD analysis contributes to our enhanced understanding of the mineralogical composition. It provides essential clues for inferring the provenance and depositional history of the Paleozoic siliciclastic sedimentary rocks along the northern Gondwana margin in the western Gulf of Suez.

Heavy mineral analysis

The analysis of heavy minerals in sedimentary petrology provides valuable insights into the composition of the source rocks of sedimentary rocks, aiding in determining origin, transport, and weathering history (Folk 1980; Chima et al. 2018). In our study, the heavy minerals were present in small quantities, constituting less than 1% of the studied sedimentary rocks. The obtained data revealed the presence of various heavy minerals. Opaque minerals such as magnetite, ilmenite, sphene, and leucoxene were identified. Additionally, ultra-stables, including zircon and rutile and metastable minerals like pyroxene and andalusite, were observed. Zircon grains in the studied samples exhibited a range of characteristics, appearing as colorless to yellow grains with euhedral, subrounded to rounded shapes, and prismatic forms with widths ranging from 200 μm to lengths of 450 μm (Fig. 4b). Some zircon crystals displayed zoning and contained inclusions such as hafnium. Zircon is an accessory mineral in igneous rocks, particularly sodium-rich plutonic rocks (Deer et al. 1966). Prismatic forms of zircon may originate from granites, according to Pettijohn et al. (1972).

Rutile grains in the samples were predominantly red and brownish red, with angular to subrounded shapes and well-developed tetragonal pyramidal terminations with dimensions ranging from 190 μm in width to 240 μm in length

(Fig. 4c). Rutile is a widely occurring accessory mineral in metamorphic rocks, especially in schists, gneisses, and amphibolites (Deer et al. 1966). Detrital rutile is predominantly sourced from high-grade regionally metamorphosed terrains, as noted by Folk (1980). Sphene grains were observed to be colorless and honey-yellow, with rounded shapes that tend towards sphericity. The outer surface of these grains displayed pits and grooves and exhibited dimensions ranging from 350 μm in width to 500 μm in length (Fig. 4d). Sphene is a common accessory mineral in igneous rocks. It is also found in ferromagnesian-rich gneisses and schists within metamorphic rocks (Deer et al. 1966).

Pyroxene fragments were identified as euhedral, angular to subangular, possibly belonging to the monoclinic form, exhibiting dimensions ranging 580 μm in width to 400 μm in length (Fig. 4e). Pyroxenes can originate from igneous or metamorphic rocks (Folk 1980). Ilmenite grains were observed as subrounded to rounded, displaying corrosion features indicative of initial to advanced stages of weathering. The grains exhibited dimensions ranging from 210 μm in width to 290 μm in length (Fig. 4f). Ilmenite is a common accessory mineral in igneous and metamorphic rocks (Deer et al. 1966).

Andalusite grains appeared colourless to pinkish tinges, angular, irregular fragments with orthorhombic prismatic shapes, and exhibiting dimensions ranging from 450 μm in width to 1200 μm in length (Fig. 4g). Andalusite is a characteristic metamorphic mineral commonly found in argillaceous rocks, gneisses, and schists (Mange and Maurer 2012). Magnetite grains in the studied sandstones exhibited a heterogeneous habit and were often associated with minerals such as potash feldspar and titanium as inclusions. The grains exhibited dimensions ranging from 800 μm in width to 620 μm in length (Fig. 4h). Magnetite is one of igneous and metamorphic rocks' most abundant oxide minerals (Deer et al. 1966).

Leucoxene grains were rounded to well-rounded in shape, exhibiting dimensions ranging from 200 μm in width to 300 μm in length (Fig. 4i). Leucoxene is a product of the alteration of ilmenite minerals (Deer et al. 1966).

Paleomagnetic data analysis

Paleomagnetic analyses were conducted to elucidate the characteristic remanent magnetizations of the Araba and Naqus formations. A series of rock magnetic experiments began with measurements of initial NRM intensities and magnetic susceptibility. The initial NRM intensities of the
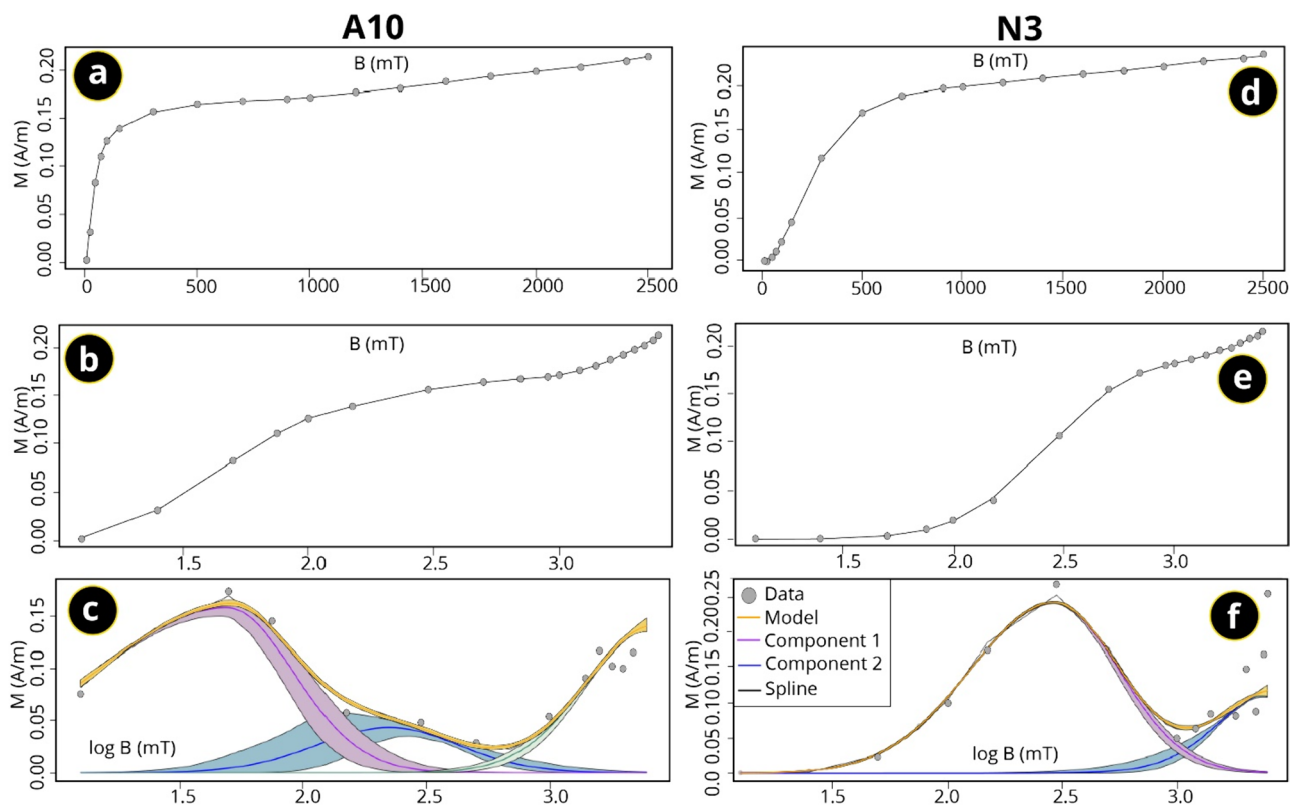
Fig. 5 Representative IRM component analysis results (Maxbauer et al. 2016) for samples from the Araba and Naqus formations. Panels **a–c** show the IRM plot, linear acquisition plot, and model fit respectively for sample A10 from the Araba Formation. Panels **d–f** present the corresponding IRM plot, linear acquisition plot, and model fit for sample N3 from the Naqus Formation. The coercivity distribu-

tions (grey circles) derived from IRM demagnetization measurements are shown, with the spline fits (partially visible as black lines). The shaded areas represent the 95% confidence intervals of the error envelopes. Where no shading is present, the confidence intervals are thinner than the lines

measured specimens from the Araba and Naqus Formations were found to range from 0.23 to 9.34 mA/m and 0.22 to 19.2 mA/m, respectively. The corresponding magnetic susceptibility values were approximately 9.47×10^{-6} SI for the Araba Formation and 28.70×10^{-6} SI for the Naqus Formation. To accurately identify and quantify the contributions from various magnetic carriers, an IRM components analysis was performed using the statistical MAX Unmix model of magnetization data, which provides the coercivity spectrum of the sample (Maxbauer et al. 2016).

The IRM acquisition curves were modeled for the sandstone specimens of the two formations with more than one component (Fig. 5a–f). The IRM acquisition curves, constructed explicitly for specimens obtained from the Araba and Naqus Formations (Fig. 5a, d), exhibited an initial rapid rate of IRM acquisition that continued slowly without reaching saturation until the maximum applied field of 2500 mT.

MAX Unmix modeling results in a three-component model for Naqus specimens (Fig. 5e, f—N3) with a primary low coercivity component (component 1) with a Bh of 1.47 (0.02) log10 units (30.10 mT) and a DP of 0.41 (0.01). The intermediate component 2 is characterized by a Bh of 2.35 (0.06) log10 units (224.4 mT) and a DP of 0.28 (0.03). A final high coercivity component 3 has a Bh of 3.57 (0.05) log10 units (3764.7 mT) and a DP of 0.37 (0.03). The low coercivity component (component 1) was identified as detrital magnetite. Components 2 and 3 are nearly identical to the hematite and goethite components, respectively.

MAX Unmix modeling results in a two-component model for Araba specimens (Fig. 5b, c—A10) with a primary low coercivity component (component 1) with a Bh of 2.39 (0.008) log10 units (248.7 mT) and a DP of 0.32 (0.004). A high coercivity component 3 has a Bh of 3.66 (0.14) log10 units (4585.3 mT) and a DP of 0.39 (0.07). The
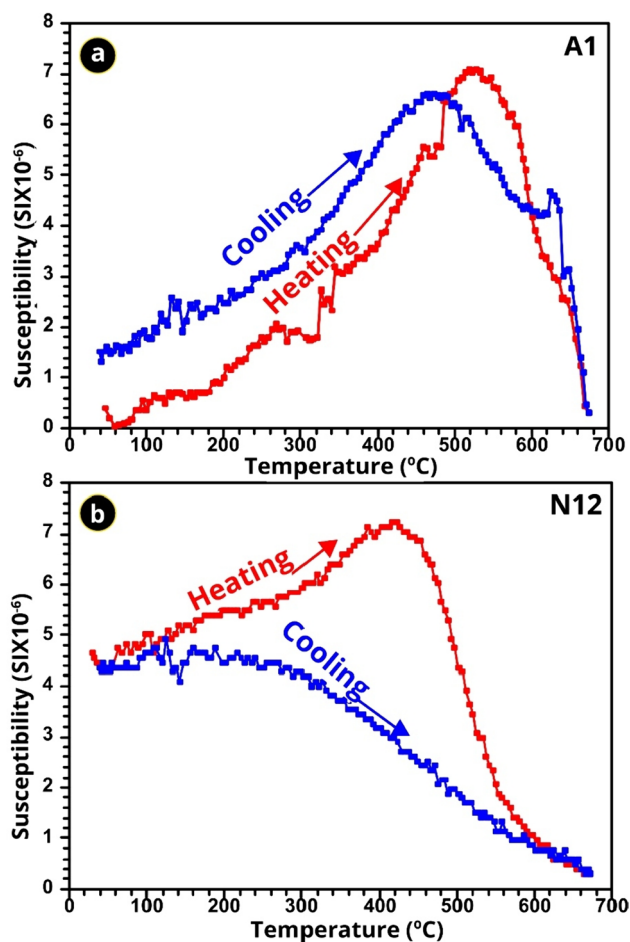
Fig. 6 Thermal dependence of magnetic susceptibility for selected samples from the Araba and Naqus formations. **a** Sample A1 from the Araba Formation shows a linear decrease in susceptibility up to approximately 580 °C, corresponding to the Curie temperature of magnetite. A small peak near 200 °C relates to the presence of goethite. A gradual decrease above 580 °C indicates some hematite. **b** Sample N12 from the Naqus Formation exhibits a more nonlinear reduction in susceptibility up to 680 °C, suggesting a mixed magnetite-hematite mineralogy. Both curves support observations of magnetite as a primary magnetic mineral, with alterations like goethite and hematite

low coercivity component (component 1) was identified as hematite. Component 2 is around the goethite component.

These observations were further supported by the susceptibility versus temperature curves (Fig. 6a, b). With the starting of the experiment, the magnetic susceptibility increases slightly upon heating, after which a drop follows at a temperature of ~580 °C, the Curie temperature of magnetite. A notable small hump displayed near ≈ 200 °C due to the

presence of goethite. A gradual decrease at temperatures $> T_c$ of magnetite indicates the presence of hematite.

Backfield curves showcased high coercivity values ranging from 280 to 320 mT (Fig. 5c). These high coercivity values suggest the presence of magnetic minerals with elevated coercivity, such as hematite and goethite, which aligns with the results of the IRM test. However, the NRM decays progressively from 200 °C and remanence is very low at the Curie temperature of hematite (Fig. 6a, b). This strongly suggests the presence of other magnetic carriers with lower unblocking temperatures, such as magnetite and ilmenite, which were identified in XRD and heavy minerals analysis.

Magnetic fabric identification

The magnetic fabrics of the Araba Formation and the Naqus Formation were characterized using AMS (Table 1 and Fig. 6a, b). The orientations of the principal axes of the AMS provide insight into the preferred alignment of ferromagnetic, paramagnetic and diamagnetic minerals, which together can result from depositional processes or subsequent deformation. The Araba Formation exhibited a high level of anisotropy (P_j) and displayed prolate AMS fabrics, as represented by the (T) values characterizing the shape of the AMS ellipsoid as prolate to oblate (Table 1 and Fig. 6a). Additional microfabric evidence supports an interpretation of primary sedimentary alignment for the Araba AMS. Observation of subrounded to angular grain shapes of magnetite under SEM (Fig. 4h) would indicate a detrital origin and preservation of the primary fabric. The presence of other detrital minerals like goethite formed through ferromagnesian mineral alteration, and kaolinite from feldspar weathering, provide further evidence of a sedimentary source. Minor hematite occurrences in some samples also point to a primary fabric. Collectively, this microfabric evidence suggests the magnetic minerals in the Araba Formation were aligned during deposition prior to diagenesis, resulting in preservation of aspects of the original sedimentary fabric structure.

Both in the Naqus and Araba formations, the maximum susceptibility axis (k_1) is subvertical and thus perpendicular or closely perpendicular to bedding, with the minimum susceptibility axis (k_3) contained within bedding. On this basis alone, it is not justified to interpret one fabric as tectonic versus the other as depositional. The observed prolate shape in the Araba Formation indicates that the particles are aligned in a manner where the k_3 is perpendicular to sedimentary layers. This alignment suggests that the magnetic fabric is likely a result of particle alignment caused by

Table 1 The combined magnetic susceptibility and AMS (anisotropy of magnetic susceptibility) data for the Araba and Naqus formations

Formation	Site	N	$K_{m\ (10^{-6}\ SI)}$	P_j	T	L	F	q	k_1 (D/I)	k_2 (D/I)	k_3 (D/I)
Naqus	N1	8	39.70	1.222	0.471	1.072	1.141	0.37	313/11	49/31	205/57
	N2	9	9.50	1.215	0.057	1.075	1.122	0.69	186/7	280/31	85/57
	N3	9	1.13	1.490	0.435	1.079	1.330	0.52	128/27	26/23	261/54
	Mean	–	28.75	1.212	0.396	1.058	1.140	0.38	–	–	–
Araba	A1	12	2.971	2.978	−0.153	1.702	0.471	0.66	175/3	270/15	38/66
	A2	11	21.81	1.498	0.027	1.282	1.125	0.71	116/41	216/12	319/46
	A3	10	2.461	3.512	0.098	0.945	1.767	0.72	317/8	104/81	226/5
	Mean	–	9.481	2.348	−0.315	1.737	1.333	0.68	–	–	–

The table includes the following information: the number of specimens (N), mean magnetic susceptibility (K_m), which is calculated as the mean of k_1, k_2, and k_3 divided by 3, and the mean eigenvectors representing the site-mean directions, including the declination and inclination of k_1 (maximum), k_2 (intermediate), and k_3 (minimum). Additional parameters provided in the table are as follows: F denotes foliation and the ratio of k_2 to k_3, L represents lineation and the ratio of k_1 to k_2, P_j indicates the corrected anisotropy degree, T represents the ellipsoid shape, and Q represents the shape parameter within the range of 0.06–0.69

Table 2 A summary of the thermal demagnetization results obtained in this study

Components	Sites	N	D (°)	I (°)	P_Lat °N	P_Long °E	α_{95} (°)	K
C_N (Naqus Formation)	N1	9	354.0	−39.9	39.0	320.8	4.1	162.36
	N2	7	335.8	−31.9	39.0	297.7	5.3	131.29
	N3	9	334.2	−40.3	33.3	299.4	4.1	220.94
	N4*	10	337.1	0.8	54.7	254.4	4.9	99.26
	Mean NSite	25	342.2	−37.8	37.8	233.1	4	61.94
C_A (Araba Formation)	A1	7	348.5	61.5	72.6	2.7	7.2	86.39
	A2	7	352.8	41.1	82.2	269.2	7.1	116.94
	A3	5	325.2	51.9	59.7	220.8	9.6	155.90
	A4	5	333.5	34.7	64.2	287.6	7.8	139.59
	A5	4	321.7	37.8	56.6	295.8	7.0	174.50
	Mean ASite	28	338.2	47.2	70.8	308.2	6.0	27.32

The key parameters included in the table are as follows: N represents the number of specimens that exhibit an isolated component, D represents the declination, I represents the inclination, α_{95} represents the radius of the 95% circle of confidence based on Fisher (1953) for the mean direction, K represents the precision parameter, and P_Lat and P_Long represent the latitude and longitude, respectively, of the virtual geomagnetic pole, * represents the site excluded from overall mean calculations for Naqus Formation. The mean values were calculated using the Remasoft 3.0 program

currents or waves during the deposition process. Supporting this interpretation, we can observe well-preserved sedimentary structures of cross-bedding that align with the fabrics at the basal part of the Araba Formation. Additionally, the sandier and thinner nature of the Araba Formation may have contributed to the preservation of the depositional fabric, with less compaction overprint. The Naqus Formation exhibited oblate AMS ellipsoids (Table 1, Fig. 6b). This oblate shape suggests the particles settled parallel to the bedding plane, with the minimum AMS axis (k_3) being vertical. The Naqus Formation may have experienced greater compaction compared to the Araba Formation due to its finer grain size

and thicker section. Some monocrystalline quartz grains in the Naqus Formation display deformation microstructures, such as slight undulose extinction, with an average modal value of 25.65% (Table 3).

Moreover, thermal demagnetization was necessary to isolate the characteristic remanent magnetization (ChRM) directions due to the presence of hematite. Stepwise thermal demagnetization was performed up to 700 °C (Table 2; Fig. 7a, b). Most samples from both formations showed a gradual decay of over 90% of their magnetization with no significant directional changes, clustering along northwest-directed positive or negative inclinations. After
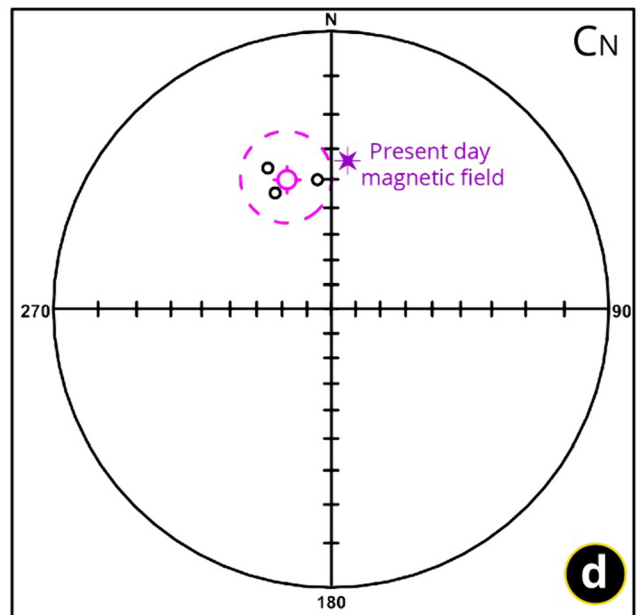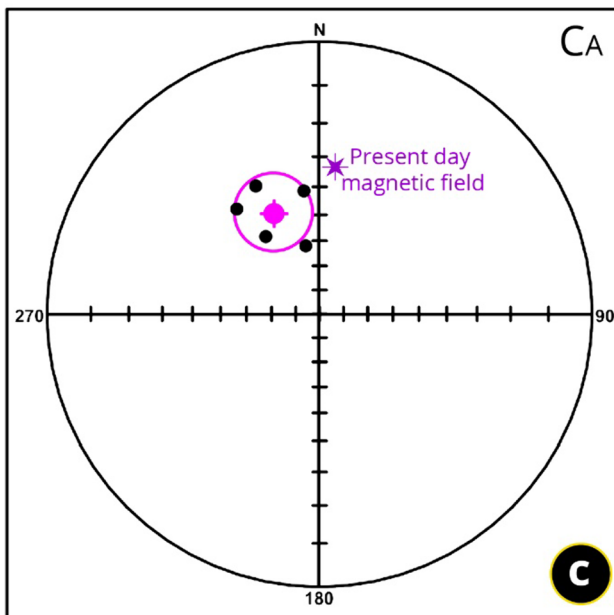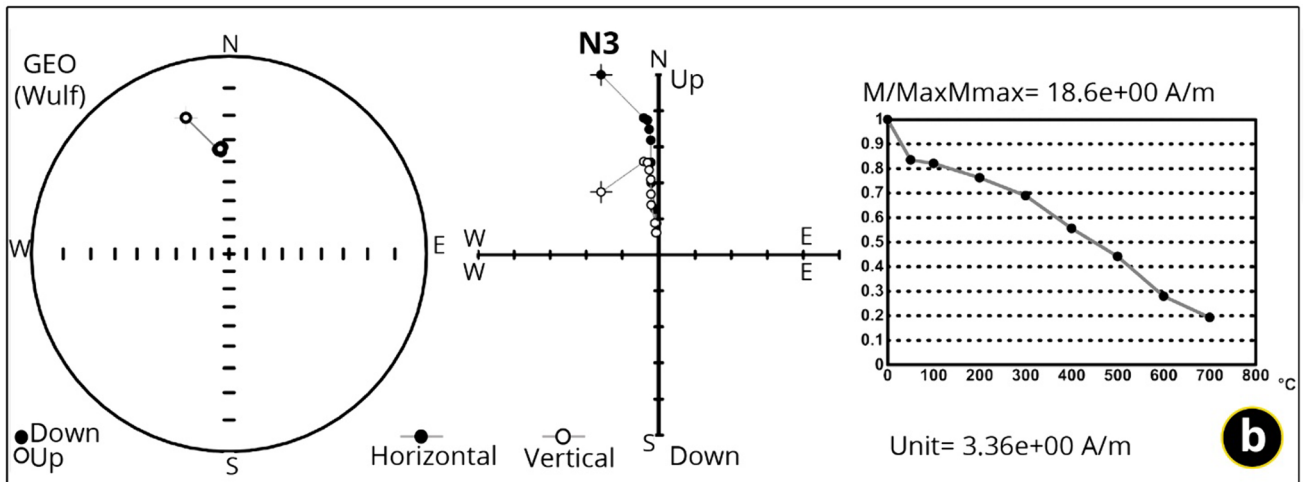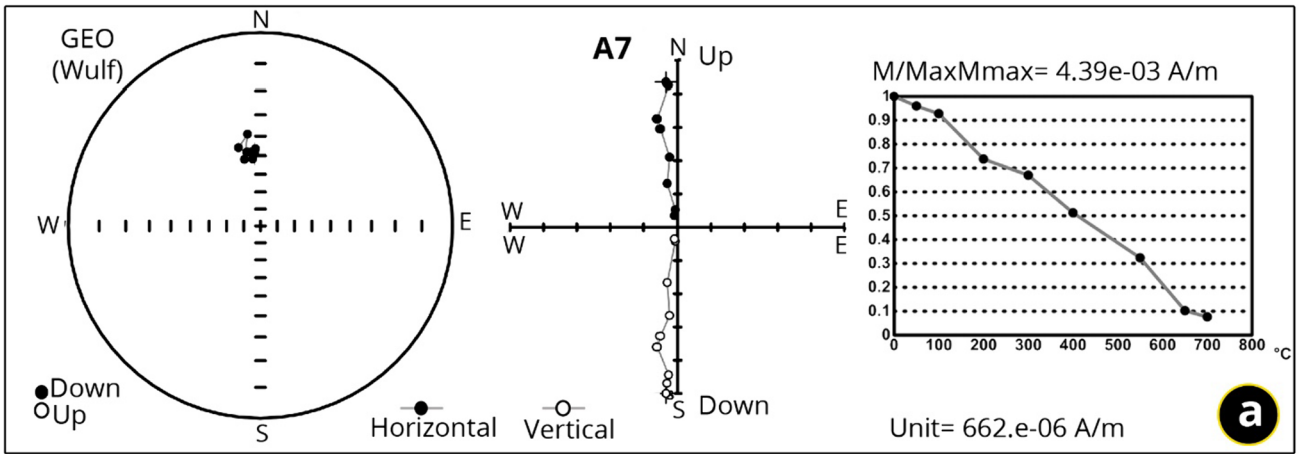
◄**Fig. 7** **a** Thermal demagnetization plots, including equal-angle stereonets and Zijderveld diagrams (Zijderveld 1967), as well as intensity decay curves, for one representative specimen (A7) from the Araba Formation. **b** Thermal demagnetization plots, including equal-angle stereonets and Zijderveld diagrams (Zijderveld 1967), as well as intensity decay curves, for one representative specimen (N3) from the Naqus Formation. **c** and **d** Equal-angle stereographic projections of site mean directions illustrating the characteristic remanent magnetization identified at the studied sites within the Araba Formation (C_A) and the Naqus Formation (C_N), along with their corresponding data mean

removal of a soft magnetic mineral component, presumed to be goethite based on XRD analysis, in initial demagnetization steps, a single remaining vector trending toward the origin of the orthogonal plot was interpreted as the primary ChRM. The goethite was effectively removed by 300 °C as evidenced by a distinct change in vector trajectory on orthogonal plots. ChRM values for individual samples typically had maximum angular deviations less than 10° below 300 °C, further supporting isolation of a stable magnetic mineral carrier (Jackson 1990; Liu et al. 2013). Principal component analysis revealed two dominant remanent magnetization components: a positive inclination component (C_A) isolated from the Araba Formation and a negative inclination component (C_N) from the overlying Naqus Formation (Fig. 7c, d). XRD and heavy mineral data detected the presence of hematite alongside other ferromagnetic minerals like goethite, magnetite, and ilmenite. IRM curves similarly indicate a mixed magnetic assemblage may carry the remanence. While hematite likely makes an important contribution, the precise mineralogical basis of these magnetization components remains ambiguous based on available characterization.

Discussion

Provenance of the Paleozoic siliciclastic sedimentary rocks

The provenance of sedimentary rocks can be elucidated by studying quartz typology and mineral inclusions in quartz crystals (Abdel-Wahab 1992; Adams et al. 2017). However, in the case of the Araba and Naqus formations, the limited presence of feldspars and rock fragments diminishes their value as reliable provenance indicators. Nonetheless, our analysis reveals that quartz characteristics play a crucial role in identifying the source rocks of the sandstones under study. Quartz occurs in both monocrystalline and polycrystalline forms. Monocrystalline quartz is a dominant component in the sandstones under study, making up an average of 85.11% and 71.42% of the Araba and Naqus formations, respectively. Most quartz grains display non-undulose extinction, which contradicts the presence of high plastic deformation strains that would typically result in undulose extinction textures. This suggests that the quartz grains have undergone minimal deformation and may have originated from a nearby source. Furthermore, these quartz grains exhibit sub-angular to subrounded shapes with low sphericity, further supporting the notion of a significant deformation overprint on the AMS fabrics. This is reinforced by the foliation mean values obtained from both formations (Table 1), which clearly indicates the presence of a pronounced deformation overprint on the AMS fabrics.

Additionally, some monocrystalline quartz grains display slightly undulose extinction, with average modal values of 13.9% for the Araba Formation and 25.65% for the Naqus Formation (Table 3). The presence of these undulose quartz grains suggests that a small proportion of the quartz grains may have undergone some degree of deformation, possibly due to transport or sedimentary processes. In summary, our analysis of quartz characteristics reveals that the Araba and Naqus formation sandstones are dominated by monocrystalline quartz with minimal deformation, suggesting a nearby source. However, the presence of some undulose quartz grains indicates that a small proportion of the quartz grains may have undergone some degree of deformation, possibly due to transport or sedimentary processes. The pronounced deformation overprint on the AMS fabrics further supports this interpretation.

The dominant detrital component in the sandstones is quartz, present in both monocrystalline and polycrystalline forms (Fig. 8). Monocrystalline quartz grains constitute a significant proportion, accounting for up to 99.01% in the Araba Formation samples and 96.38% in the Naqus Formation samples (Table 3). This dominance indicates that the sedimentary rocks primarily originated from plutonic sources (Blatt 1967; Folk 1974), particularly granitic rocks (Basu et al. 1975). The detrital framework grains of the Araba and Naqus samples commonly contain heavy minerals, including zircon (Fig. 8a), rutile (Fig. 8b), sphene (Fig. 8c), allanite (Fig. 8d), muscovite (Fig. 8e), and epidote (Fig. 8f). Additionally, the presence of biotite inclusions (Fig. 8g) indicates the presence of metamorphic rocks, which are commonly found in gneisses and greenschists.

Table 3 The estimated mineralogical composition obtained from modal analysis of the Araba and Naqus formations' sandstones

Sample no.	Grain size	Sorting	Rounding	Total quartz %	Monocrystalline quartz (Q_m) %		Polycrystalline Quartz (Q_p) %	Feldspars (F) %	Lithic fragments (L) %	Heavy mineral fractions %	Mica
					undulatory extinction %	Non-undulatory extinction %					
N 8	F	V.W	SR	99.2	13.66	82.12	4.21	0.65	0	0.15	0
N 7	F	M	SA-SR	99.4	21	75.96	3.04	0	0	0.19	0.39
N 6	F	M	SA-SR	98.95	27.01	69.36	3.63	0.41	0	0.21	0.41
N 4	F	W	SA-SR	99.58	27.9	69.2	2.9	0	0	0.42	0
N 3	V.F	M	SA-SR	98.9	31.59	66.14	2.27	0	0	0.18	0.92
N 2	V.F	W	SA-SR	99.71	29.58	68.34	2.08	0	0	0.29	0
N 1	F	V.W	SR	99.55	28.81	67.57	3.62	0	0	0.15	0.3
Average				99.32	25.65	71.24	3.1	0.15	0	0.22	0.28
A 10	V.F-F	M	SA-SR	99.66	11.67	88.33	0	0	0	0	0.33
A 9	V.F-C	P	SA-SR	99.61	16.28	81.76	1.96	0	0	0.39	0
A 8	S.S	P	VA	99.68	9.23	90.77	0	0.2	0	0.12	0
A 7	V.F	P	SA	99.93	12.41	87.58	0	0	0	0	0.07
A 6	V.F	M	SA	97.3	11.8	86.62	1.58	0	0	0.15	2.55
A 3	M-C	M	SA	91.24	19.23	78.85	1.92	3.5	5.26	0	0
A 2	V.F	M	SA-SR	97.81	16.74	81.86	1.39	0.27	0.36	1.56	0
Average				97.89	13.9	85.11	0.97	0.56	0.8	0.31	0.42

S.S silt-sized grains, *V.F* very fine-grained grains, *F* fine-grained grains, *V.F-F* very fine to fine grained, *M-C* grains ranging from medium to coarse grained, *V.F-C* grains ranging from very fine to coarse grained, *V.W* very well-sorted grains, *W* well-sorted grains, *M* moderately-sorted grains, *P* poorly-sorted grains, *VA* very angular grains, *SA* represents sub-angular grains, *SA-SR* grains ranging from sub-angular to sub-rounded, *SR* sub-rounded grains

Therefore, it is plausible that quartz grains with diverse mineral inclusions could have originated from a gneiss source.

Other types of inclusions, such as apatite inclusions (Fig. 8h), may suggest the presence of igneous rocks (Deer et al. 1966). These specific heavy minerals provide further insights into the type of source area or provenance, indicating igneous and metamorphic origins. Field observations reveal that the Wadi Dakhl area under study is encompassed by an abundance of granitic and metavolcanic rocks from the Precambrian Supereon (Fig. 2a). This observation strongly suggests that the sandstones analyzed in this study might have originated from these nearby crystalline formations.

Polycrystalline quartz grains represent a smaller proportion, accounting for up to 0.97% of the total framework in the Araba Formation and 3.1% in the Naqus Formation (Table 3). The characteristics of polycrystalline quartz are instrumental in distinguishing between igneous and metamorphic origins. Sutured boundaries between crystals indicate a metamorphic origin, while straight boundaries suggest an igneous origin (Adams et al. 2017). In the Araba Formation, the observed polycrystalline quartz grains consist of two crystals with straight to slightly curved intercrystalline boundaries, a characteristic commonly associated with a plutonic origin (Fig. 8i). On the other hand, the polycrystalline quartz grains within the Naqus Formation exhibit multiple crystals that exhibit both straight and curved sutures. These crystals are distinguished by the number of extinctions, with counts of 3 (Fig. 8j), 5 (Fig. 8l), or even exceeding 10 (Fig. 8m, n). A few quartz grains in the Naqus Formation consist of two crystals with straight contacts. These observations suggest that most of the polycrystalline quartz grains in the study area were derived from the surrounding metamorphic rocks. Specifically, monocrystalline and polycrystalline quartz grains with elongated or platy shapes are characteristic of quartz derived from schistose formations, as noted by Folk (1980). Such monocrystalline quartz grains are documented in the Naqus Formation (Fig. 8k). The orientation of these derived elongated quartz crystals from the metamorphic rocks (Fig. 8j, n) provides evidence of compaction through metamorphism.

Furthermore, elongated crystals with straight to concave–convex-shaped boundaries in the studied polycrystalline quartz grains further support a metamorphic origin (Ekwenye et al. 2015). The dominance of monocrystalline quartz grains suggests a plutonic origin, possibly from granitic sources. At the same time, the presence of specific heavy minerals indicates the presence of both igneous and metamorphic source rocks. Observing polycrystalline quartz grains with distinct boundary characteristics further aids in distinguishing between igneous and metamorphic origins. Moreover, the provenance of the Paleozoic siliciclastic sedimentary rocks was also elucidated using AMS analysis. Magnetic fabric characteristics revealed by AMS measurements provided insights into depositional and post-depositional processes recorded in the Araba and Naqus formations. The Araba Formation displayed a high degree of anisotropy with predominantly subvertical k_1 orientations perpendicular to bedding and k_3 contained within bedding, indicative of a depositional and/or early tectonic overprint. AMS ellipsoids showed a wide shape distribution from oblate to prolate. Similarly, AMS ellipsoids for the Naqus Formation exhibited subvertical k_1 axes perpendicular or closely perpendicular to bedding with k_3 contained within bedding, consistent with commonly observed compaction fabrics. Overall, integrated AMS and petrographic evidence suggested depositional/compaction signals overprinted by a subsequent regional structural overprint in both formations. AMS analysis further revealed a clear clustering of maximum axes in the northwest–southeast direction. This orientation indicates modification of an original depositional fabric by the prevalent Cenozoic extensional tectonism in the Gulf of Suez region (Tables 4 and 5).

Additionally, the XRD data support the petrographic observations, confirming the dominant presence of quartz arenite in both the Araba and Naqus formations. However, it is the identification of specific accessory minerals that provides valuable insights into the subtle variations in provenance between these formations. Minerals such as goethite, kaolinite, and hematite were identified in samples from the Araba Formation through XRD analysis. Notably, calcite was exclusively found in Araba Formation samples and not in those from the Naqus Formation. The Naqus Formation samples yielded additional minerals including anatase, microcline, and halite. The mineral assemblages in the Araba Formation point to a predominantly igneous source with minimal marine influence. In contrast, the Naqus Formation tells a different story, indicating a mixed origin derived from igneous and metamorphic sources. These mixed sources can be attributed to the unique depositional environment within evaporitic coastal plains. The presence of both igneous and metamorphic sources in the Naqus Formation signifies a broader range of rock types contributing to the sedimentary material compared to the predominantly
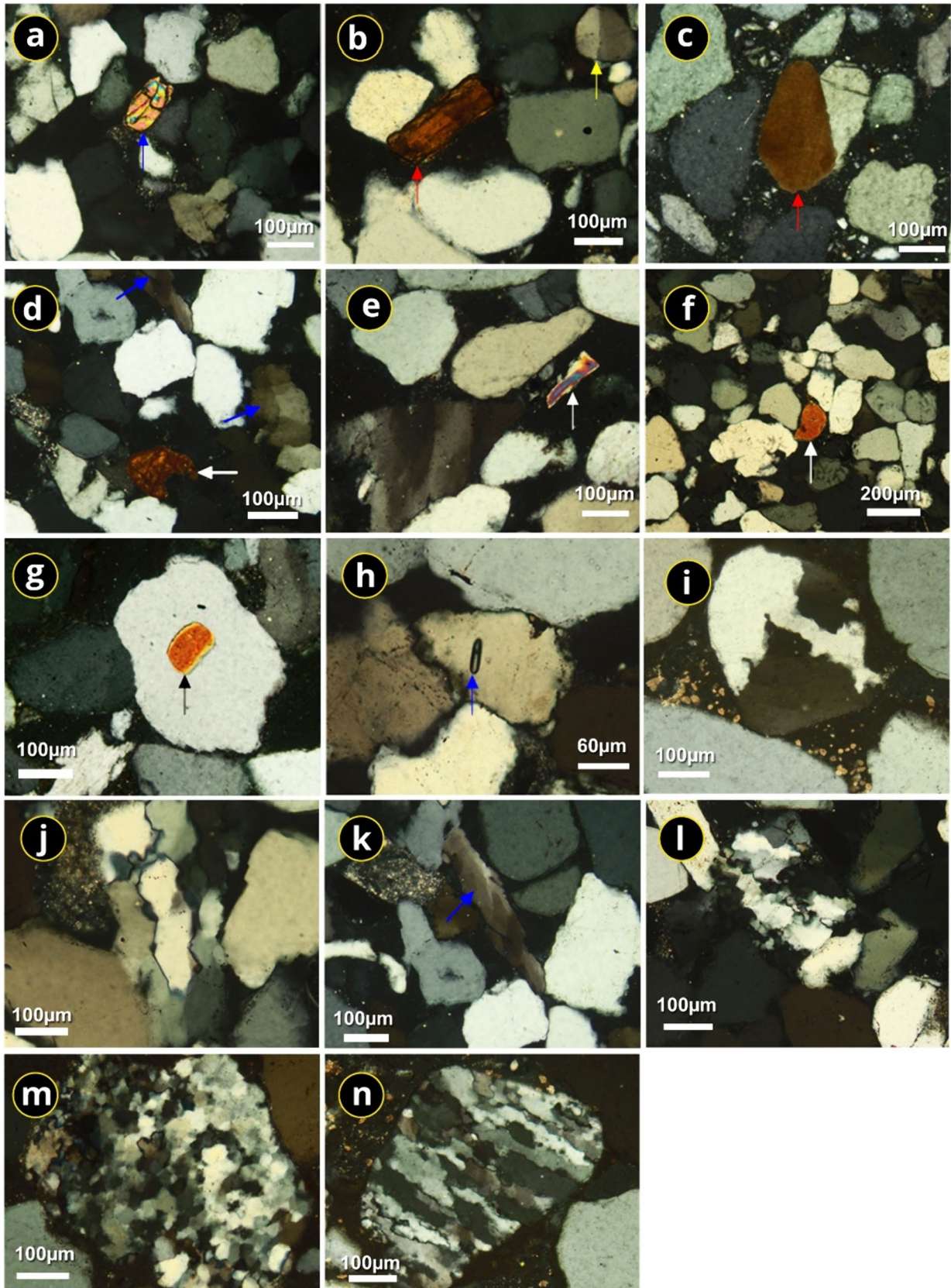
◄**Fig. 8** Photomicrographs provide detailed visual representations of various quartz grains, mineral inclusions, and crystal characteristics from both the Araba and Naqus formations, shedding light on their origins and compositions. **a** Monocrystalline detrital quartz with detrital zircon (blue arrow) from the Naqus Formation. **b** Rutile grains (red arrow) and a polycrystalline quartz grain consisting of two crystals with a straight intercrystalline boundary (yellow arrow) from the Naqus Formation. **c** Monocrystalline detrital quartz displaying straight extinction with sphene (red arrow) from the Araba Formation. **d** Allanite mineral (white arrow) and a strained quartz grain (blue arrows) from the Naqus Formation. **e** Detrital muscovite flakes (white arrow) and a strained quartz grain (black arrow) from the Naqus Formation. **f** Epidote grain (white arrow) from the Naqus Formation. **g** Biotite inclusion in monocrystalline detrital quartz (black arrow) from the Araba Formation. **h** Apatite inclusion in a monocrystalline detrital quartz (blue arrow) from the Naqus Formation. Additionally, the figure includes photomicrographs of polycrystalline detrital quartz grains from both the studied Araba (**i**) and Naqus (**j–n**) formations: **i** Polycrystalline quartz grain consisting of two crystals with straight to slightly curved intercrystalline boundaries (plutonic origin). **j** Polycrystalline quartz grain consisting of three crystals with sutured crystal-crystal boundaries. **k** Strained monocrystalline quartz grain (blue arrow) with elongated crystals indicating either a schistose or hydrothermal origin, characteristic of metamorphic origin. **l** Polycrystalline quartz grain with concave–convex shaped boundaries (metamorphic origin). **m** Polycrystalline quartz with numerous silt-size individual crystals (metamorphic origin). **n** Polycrystalline quartz with sutured crystal-crystal boundaries and almost perfect orientation of elongated and crenulated crystals (metamorphic origin)

igneous source observed in the Araba Formation. This complexity in provenance suggests a more intricate origin and hints at a more dynamic depositional environment. It implies that the sedimentary rocks in the Naqus Formation were deposited in a setting influenced by a combination of tectonic, climatic, and environmental factors, with the evaporitic coastal plains playing a significant role.

Age determination

The age determination of the Araba and Naqus formations in the western Gulf of Suez was primarily carried out using paleomagnetism. Analysis of the ChRM directions provided a means for dating by allowing comparison to variations in the geomagnetic field over time. Paleomagnetic analysis of the ChRM directions in the formations served to date them by correlating the recorded magnetic signals to established geomagnetic polarity timescales. The accuracy of the resulting paleomagnetic records is supported by the stability of NRM intensities during stepwise thermal demagnetization experiments. The magnetic susceptibility values for the Araba and Naqus formations were approximately 9.47×10^{-6} SI and 28.70×10^{-6} SI, respectively. The high

IRM values in these samples indicate the presence of high-coercivity magnetic minerals, particularly hematite, carrying the remanence. However, the magnetic susceptibility versus temperature curves exhibits significant susceptibility decays at a temperature of ~ 580 °C, the Curie temperature of magnetite (Fig. 6a, b), which is closer to the Curie temperature of magnetite. Additionally, a small hump was observed around 200 °C, which can be attributed to the presence of goethite. A gradual decline in remanence is seen at temperatures greater than the Curie temperature of magnetite, indicating the presence of hematite.

Furthermore, the thermal demagnetization curve showing a decrease around 680°C confirms the presence of hematite but does not rule out a mixed magnetic mineralogy that includes magnetite, given the earlier susceptibility decay observed in some samples. Overall, the IRM results suggest that hematite may be the dominant ferromagnetic carrier in these samples, but the presence of goethite, magnetite and ilmenite cannot be ruled out due to the observed susceptibility decays and the mixed magnetic mineralogy. AMS analysis revealed distinct magnetic fabric characteristics between the Araba and Naqus formations. The Araba Formation displayed a high degree of anisotropy (P_j) with predominantly subvertical k1orientations perpendicular to bedding and k3 contained within bedding (Fig. 9a). Comparison of K_m values against corrected P_j showed a negative correlation, indicating P_j values were not influenced by mineralogical variations but rather reflect deformation-related petrofabric suitable for structural interpretation (Fig. 9c, g). This alignment could reflect depositional processes like compaction or currents/waves during deposition, or an earlier tectonic overprint. AMS ellipsoids for the Araba Formation showed a wide shape parameter distribution from oblate to prolate ($-1 < T < 1$; Fig. 9). Notably, P_j values exceeded 1.05, outside the range expected for purely paramagnetic assemblages (Fig. 9b, f, d, h).

Similarly, AMS ellipsoids for the Naqus Formation exhibited subvertical k_1 axes perpendicular or closely perpendicular to bedding with k_3 contained within bedding (Fig. 9d). This orientation is consistent with commonly observed compaction-imparted fabrics in sedimentary strata. The observed clustering in the NW–SE direction of the maximum AMS axes in both the Araba and Naqus formations suggests the presence of a primary depositional fabric that was subsequently modified by tectonic deformation. The consistent alignment of the maximum axes of AMS in the Araba and Naqus formations suggests that this fabric developed during a regional tectonic event. The differences observed between

Table 4 A comprehensive overview of the frequency distribution of heavy minerals within the studied Paleozoic sandstones

Formation	Sample No	Zircon	Rutile	Sphene	Magnetite	Ilmenite	leucoxene	Pyroxene	Andalusite
Naqus	N8	0.00	78.5	0.00	0.00	0.00	0.00	21.5	0.00
	N7	15.8	49.6	0.00	17.56	0.00	0.00	0.00	17.04
	N6	0.00	48.32	0.00	0.00	18.96	15.58	0.00	17.14
	N2	0.00	0.00	0.00	0.00	0.00	0.00	0.00	100
	N1	0.00	0.00	0.00	0.00	100	0.00	0.00	0.00
Araba	A9	0.00	0.00	0.00	0.00	23.9	26.4	49.7	0.00
	A2	14.56	0.00	16	0.00	40.85	0.00	28.57	0.00

This information is crucial for understanding the sedimentary processes, provenance, and depositional history of the studied sandstone units

Table 5 A compilation of selected paleomagnetic pole positions for Africa and Egypt during the Paleozoic period (419–360 Ma)

Pole no.	Region, rock unit	Age (Ma)	Paleopole position P_Lat	P_Long	A_{95} or dp/dm	References
Egypt						
1	SW Sinai: Abu Durba Sandstone-B	Upper Carboniferous, (Re)	25.6	244.0	7.1	Abdeldayem et al. (1994)
2	Eastern Desert: Esh El Mellaha dikes-Intm	431 Ma, (R)	81.6	120.8	3.3/5.2	Abdullah et al. (1984)
3	Eastern Desert: Um-Rus Dikes	481 ± 17 Ma, (R)	86	193	6.2/5.4	Davies et al. (1980)
4	Eastern Desert: Esh El Mellaha Dikes-A	500 Ma, (R)	87.3	25.9	9.6/14.5	Abdullah et al. (1984)
5	Eastern Desert: Qena-Safaga Dikes	504 ± 24 Ma, (R)	87.3	304.2	5.0/4.8	Davies et al. (1980)
6	Eastern Desert: Esh El Mellaha Dikes- B	532 Ma, (R)	82.7	266.5	5.6/9.1	Abdullah et al. (1984)
7	SW Sinai: Abu Durba Sandstone-A	Cambrian, (Re)	18	341	44.9	Abdeldayem et al. (1994)
8	Eastern Desert: Hammamat sediments	Cambrian, (Re)	74	310	11	Abdeldayem et al. (2004)
9	Southwestern desert: Bir Safsaf Dikes	Cambrian, (Re)	80	249.7	9.2	Saradeth et al. (1989)
10	Eastern Desert: Um Rus Dikes	Early Paleozoic, (Re)	87	164	5	Saleh (2020)
11	Red Sea: Qena, Post Hammamat felsite	Proterozoic-Cambrian, (Re)	38	325	23	Abdel-Al et al. (2001)
12	Eastern Desert: Ras Gharib Dikes	Proterozoic-Cambrian, (Re)	75	339	6	Hare and Nairn (1990)
13	Eastern Desert: Younger Granites	Proterozoic-Cambrian, (Re)	82	244.8	11/19	Nairn et al. (1987)
14	Eastern Desert: Wadi El-Dakhal, Araba Fm (CA)	Cambrian, (Re)	70.8	308.2	6	This study
15	Eastern Desert: Wadi El-Dakhal, Naqus Fm (CN)	Carboniferous, (Re)	37.8	233.1	4	This study
Africa						
16	Algeria: Hassi- Bachir	Upper Carboniferous, (Re)	32.8	235.7	3.7	Derder et al. (2009)
17	Algeria: Ain-Ech Chebbi	Upper Carboniferous, (Re)	26.5	224.7	4.7	Derder et al. (2001a)
18	Algeria: In Ezzane	Upper Carboniferous, (Re)	25.2	239.9	5.4	Amenna et al. (2014)
19	Morocco: Carboniferous LS	Upper Carboniferous, (Re)	7.4	234.5	11.0	Salmon et al. (1988)
20	Morocco: Carboniferous rocks	Upper Carboniferous, (Re)	4.8	235.5	6.1	Martin et al. (1978)
21	Sudan: Sabaloka Complex	Lower Carboniferous, (Re)	42.0	235.7	7.0	Soffel et al. (1990)
22	Algeria: Intrusive doleritic rocks	347.6 ± 8.1 Ma, (R)	36.3	233.6	5.2	Derder et al. (2006)
23	Sudan: Gilif Hills volcanics	377 ± 5 Ma, (R)	25.9	191.6	10.8	Bachtadse and Briden (1991)
24	South Africa: Graafwater Fm	400 Ma, (R)	28	194	8.8	Bachtadse et al. (1987)
25	Sudan: Salala Complex	463 Ma, (R)	39.6	329.5	9.3	Bachtadse and Briden (1989)
26	Namibia: Blaubeker formation	471 ± 26 Ma, (K–Ar)	51.0	352.0	10/21	Kroner et al. (1980)
27	Zambia: Hook batholith	500 ± 17 Ma	14	336.5	36	Brock (1967)
28	Malawi: Ntonya ring Structure	522 ± 13 Ma	27.7	344.9	1.4/2.3	Briden (1968)
29	Sudan: Sabaloka ring complex	540 ± 25 Ma, (K–Ar)	83	339.0	10	Briden (1973)
30	Sudan: Nabati Complex	Cambrian	67.9	314.1	13.6	Saradeth et al. (1989)

the formations may be attributed to the localization of deformation along pre-existing weaknesses. The NW–SE orientation of the AMS lineations is likely a result of the extensional tectonic activity prevalent in the region during the Cenozoic. The positive inclination overprints observed in the AMS data are consistent with remagnetizations, which are believed to be linked to large-scale fluid flow and heating during the Afro-Arabian rifting associated with the opening of the Red Sea and the Gulf of Suez.

The demagnetization results in Table 2 show that the site-mean directions of samples from the Araba Formation clearly group towards the northwest, with moderately positive inclinations. The overall mean direction for this positive polarity component across all Araba Formation sites is a declination of 338.2° and inclination of 47.2°, with an α_{95} value of 6°. The corresponding virtual geomagnetic pole lies at 70.8° N latitude and 308.2° E longitude. Similarly, the site-mean directions of samples from the Naqus Formation also exhibit a clear northwestward grouping but with moderately negative inclinations. The overall mean direction for the negative polarity component spanning three Naqus Formation sites is a declination of 342.2° and inclination of −37.9°, having an α_{95} value of 4°. This places the associated virtual geomagnetic pole at 37.8° N latitude and 233.1° E longitude (Fig. 7c, d). However, it is important to note that samples from the Naqus site N4 display a dual polarity magnetization. It is worth noting that the Naqus Formation site N4 samples were collected along a different level compared to the other Naqus Formation sites. The mean direction of 254.4° declination and 54.7° inclination of this component differs significantly from the other Naqus Formation components and aligns near Cretaceous paleomagnetic poles. This may suggest that the site N4 samples represent a remagnetized interval within the Naqus Formation. The similarity of this component's mean direction to the Araba Formation samples, which were collected along the same level, may indicate a common depositional or tectonic history for these formations.

The reliability of our paleomagnetic components was evaluated based on the quality criteria proposed by Van der Voo (1990) and updated by Meert et al. (2020). These criteria examine seven factors: well-determined rock age, adequate sample sizes and statistical precision, suitable demagnetization techniques, applicable field tests, consideration of structural control, presence of dual polarity magnetization, and confirmation of primary magnetization. While our Araba and Naqus poles satisfy criteria regarding sample sizes, statistical precision, and demagnetization techniques,

they lack known age constraints. Furthermore, the Naqus Formation site N4 samples displayed a dual magnetization, whereas no reversed polarities were identified within the other study sites at the site scale, partially fulfilling another criterion of antipodal dual polarities pointing to a primary magnetization. However, as noted above, the N4 samples were not from the same stratigraphic level as the other Naqus Formation sites characterized. Additionally, components C_A and C_N from both formations show significant divergence from the present-day field according to the IGRF model. However, it is important to note that remagnetization can occur over an extended period, from the Paleozoic to the present.

To provide a general overview and tentative interpretation, we plotted the resultant VGPs (C_A and C_N) alongside 30 previously published paleopoles from Egypt and Africa with reliable age constraints derived from radiometric dating techniques (R–Sr, U–Pb, K–Ar). These published poles represent the expected paleomagnetic field orientations for different geological periods. The comparison reveals consistency between pole C_A obtained from the Araba Formation and Paleozoic (Cambrian Period) poles reported by (Abdullah et al. (1984) and Abdeldayem (2003), suggesting a similar magnetization age. Similarly, pole C_N obtained from the Naqus Formation shows consistency with radiometrically dated Carboniferous poles reported by Derder et al. (2006), indicating a comparable magnetization age. However, when plotted against the most recent Gondwana Apparent Polar Wander Path (APWP) by Torsvik et al. (2012) in southern African coordinates, pole C_A clusters around the Cenozoic–Mesozoic portion (60–80 Ma), inconsistent with the inferred age (Fig. 10). In contrast, pole C_N aligns well with the late Paleozoic section (300–320 Ma) of the Torsvik curve (Fig. 10). The Mesozoic positioning of pole C_A could reflect remagnetization associated with large-scale tectonic events like the breakup of Pangea and closure of the Tethys Sea. Similar widespread Late Paleozoic remagnetization has been proposed for the West African craton by Perrin and Prévot (1988).

Considering a positive inclination component (C_A) in the Araba Formation and a negative inclination component (C_N) in the overlying Naqus Formation, it can be inferred that the deposition of the Araba and Naqus formations occurred during a prolonged interval of reverse polarity. The paleogeographic position of the considered area in the southern hemisphere during the Paleozoic Era (Fig. 1a, b) suggests that the positive inclination fabric observed in both formations could potentially indicate preserved primary inclinations
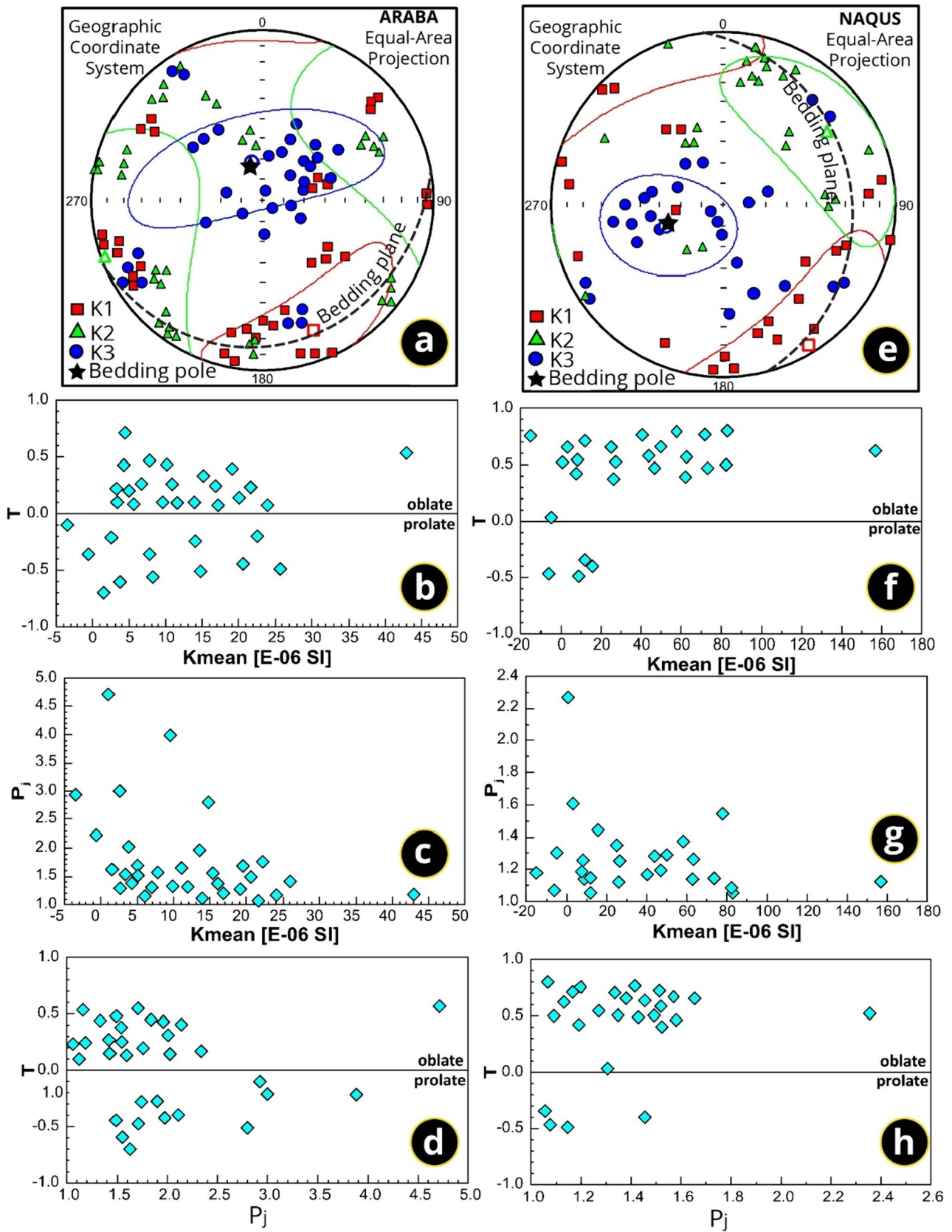
Fig. 9 **a** An equal-area projection illustrating the in situ directions of magnetic susceptibility principal axes for sites within the Araba Formation. **b** The plots depict the relationships between susceptibility (K_m) and corrected anisotropy degree (P_j) for the Araba Formation. **c** The plot represents the relationships between susceptibility (K_m) and shape parameter (T) for the Araba Formation. **d** An equal-area projection visualizing the in situ directions of magnetic susceptibility principal axes for sites within the Naqus Formation. **e** The plots demonstrate the relationships between susceptibility (K_m) and corrected anisotropy degree (P_j) for the Naqus Formation. **f** The plots showcase the relationships between susceptibility (K_m) and shape parameter (T) for the Naqus Formation. The dotted arc represents the bedding plane. The black star indicates a sedimentary bedding pole

related to the changing paleogeography during deposition in northern Gondwana (Fig. 9a, e). Correlating these polarity orientations to the geomagnetic polarity timescale allowed age constraints to be placed on deposition (Fig. 10).

Specifically, the positive component C_A suggested deposition of the Araba Formation during the Cambrian Period. However, later remagnetization of the Araba Formation during the Carboniferous period cannot be ruled out based on available evidence. Meanwhile, the negative component C_N indicated the Naqus Formation deposited during the Carboniferous Period. This magnetostratigraphic correlation provides the first reliable depositional ages determined for the Araba and Naqus formations. It critically constrains the Araba Formation to the Cambrian and Naqus Formation to the Carboniferous, establishing an important chronostratigraphic framework for these units previously lacking firm age control. Such age determination offers valuable chronostratigraphic control, enriching our understanding of the Paleozoic siliciclastic sedimentary rocks along the northern Gondwana margin in the western Gulf of Suez.

Conclusions

Petrographic analysis of the sandstones and siltstones identified various microfacies, indicating varied maturity and sediment sources. Heavy mineral analysis recognized specific heavy minerals suggesting mixed igneous and metamorphic sources. X-ray diffraction analysis revealed the siliciclastic rocks contain quartz, goethite, kaolinite, and lesser hematite. Paleomagnetic dating isolated two distinct components: one associated with the Cambrian period dated the Araba Formation (C_A), while another linked to the Carboniferous period (C_N) corresponded to the Naqus Formation. AMS data also indicated a primary depositional fabric and subsequent tectonic deformation characterized by NW–SE extension in the studied formations. These findings provide insights into the provenance, suggesting a predominantly intracratonic basin setting with sediment recycling from the uplifted Arabian-Nubian shield. Key uncertainties regarding the formations' ages and provenance are thus resolved.
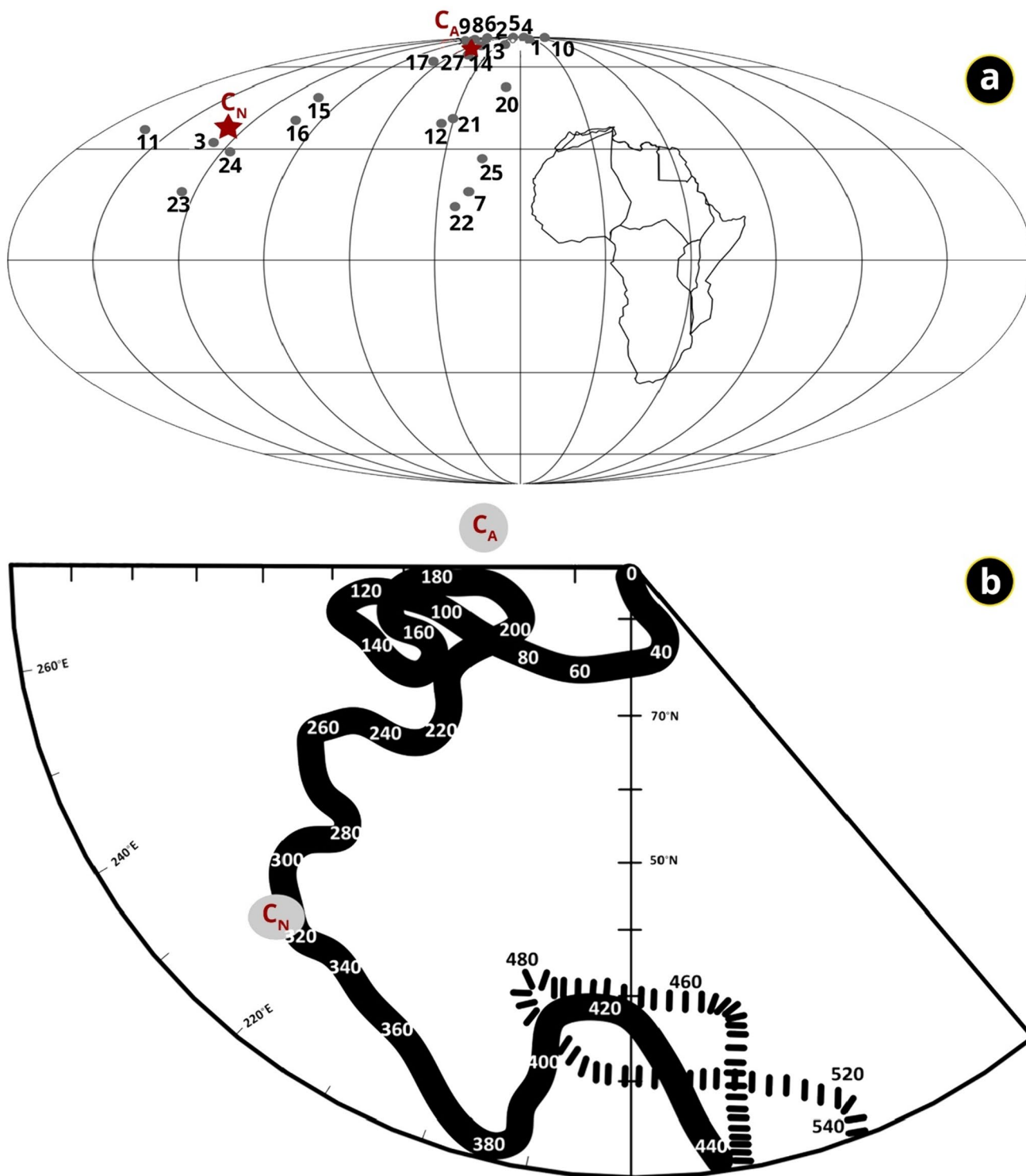
Fig. 10 **a** Comparison of Paleozoic paleomagnetic poles from Egypt and Africa published in previous studies with the poles obtained in the current study (represented by red stars). **b** Comparison of Pale-ozoic paleomagnetic poles (C_A and C_N) (shown as gray ovals) with Torsvik's APWP (depicted as a black line)

Declarations

Conflict of interest The authors confirm that any potential conflicts of

References

Abdallah AM, Darwish M, El Aref M, Helba AA (1992) Lithostratigraphy of the Pre-Cenomanian clastics of North Wadi Qena, Eastern Desert, Egypt. In: Sade A (ed) Proceedings of the first international conference on geology of the Arab World, Cairo University, pp 255–282

Abd El-Wahed M, Attia M (2023) Structural and tectonic evolution of suture-related belts and post-accretionary systems in the Arabian-Nubian Shield. Geol J 58:1776–1809. https://doi.org/10.1002/gj.4693

Abdeldayem AL (2003) Paleomagnetic dating of the Gebel El -Zite Paleolozoic sandstone, SW Gulf of Suez. Egypt Egypt J Geol 47:361–375

Abdeldayem AL, Kafafy AM, Tarling DH (1994) Palaeomagnetic studies of some Palaeozoic sediments, southwest Sinai, Egypt. Tectonophysics 234:217–225. https://doi.org/10.1016/0040-1951(94)90212-7

Abdeldayem AL, Kafafy AM, ElSayed RA (2004) Paleomagnetism of the Hammamat rocks and younger granite of Gabal Qattar area, northern Eastern Desert, Egypt. Annu Geol Surv Egypt 27:317–334

Abdel-All E, Lofty HI, El Habak G (2001) Remagnetization of the Late Precambrian rocks in the Fawakhir area, central eastern desert of Egypt: a paleomagnetic study on four pan-African rock units. JPME 4:1–34

Abdelfadil KM, Mahdy NM, Ondrejka M, Putiš M (2022) Mineral chemistry and monazite chemical Th–U–total Pb dating of the Wadi Muweilha muscovite pegmatite, Central Eastern Desert of Egypt: constraints on its origin and geodynamic evolution relative to the Arabian Nubian Shield. Int J Earth Sci 111:823–860. https://doi.org/10.1007/s00531-021-02152-3

Abd-Elhameed S, Mahmoud A, Salama Y (2021) Late Moscovian phylloid algal-microbial mounds from Wadi Araba, north Eastern Desert, Egypt: a new construction model and paleogeographic distribution. Int J Earth Sci 110:3001–3013. https://doi.org/10.1007/s00531-021-02097-7

Abdel-Rahman A-FM, Martin RF (1987) Late Pan-African magmatism and crustal development in northeastern Egypt. Geol J 22:281–301. https://doi.org/10.1002/gj.3350220403

Abdel-Wahab AA (1992) Provenance of Gebel El-Zeit sandstones, gulf of Suez, Egypt. Sediment Geol 75:241–255. https://doi.org/10.1016/0037-0738(92)90095-9

Abdullah A, Nairn AEM, Savino D, Sprague K (1984) Paleomagnetic study of some of the dikes from the Esh El Mellaha Range, Eastern Desert, Egypt. J Afr Earth Sci 2:267–275

Adams AE, Mackenzie WS, Guilford C (2017) Atlas of sedimentary rocks under the microscope. Routledge

Afanas'yev GD, Bagdasaryan GP, Garris MA, Khramrabayev IK (1965) Basic data on the age of the boundaries between certain geological systems and epochs. Int Geol Rev 7:1928–1948. https://doi.org/10.1080/00206816509474168

Ali KA, Stern RJ, Manton WI et al (2010) Neoproterozoic diamictite in the Eastern Desert of Egypt and Northern Saudi Arabia: evidence of ~750 Ma glaciation in the Arabian-Nubian Shield? Int J Earth Sci 99:705–726. https://doi.org/10.1007/s00531-009-0427-3

Allam A (1989) The Paleozoic sandstones in Wadi Feiran—El Tor area, Sinai, Egypt. J Afr Earth Sci 9:49–57. https://doi.org/10.1016/0899-5362(89)90007-9

Amenna M, Derder MEM, Henry B, et al (2014) Improved Moscovian part of the Gondwana APWP for paleocontinental reconstructions, obtained from a first paleomagnetic pole, age-constrained by a fold test, from In Ezzane area in the Murzuq basin (Algeria, stable Africa). J African Earth Sci 99:342–352

Andresen A, Abu El-Enen MM, Stern RJ et al (2014) The Wadi Zaghra metasedimentary rocks of Sinai, Egypt: new constraints on the late Cryogenian-Ediacaran tectonic evolution of the northernmost Arabian-Nubian Shield. Int Geol Rev 56:1020–1038. https://doi.org/10.1080/00206814.2014.907755

Bachtadse V, Briden JC (1991) Palaeomagnetism of Devonian ring complexes from the Bayuda Desert, Sudan—new constraints on the apparent polar wander path for Gondwanaland. Geophys J Int 104:635–646

Bachtadse V, Van der Voo R, Hälbich IW (1987) Paleomagnetism of the western Cape Fold belt, South Africa, and its bearing on the Paleozoic apparent polar wander path for Gondwana. Earth Planet Sci Lett 84:487–499

Bachtadse V, Briden JC (1989) Palaeomagnetism of the Early to Mid-Ordovician Salala igneous complex, Red Sea Hills, Sudan. Geophys J Int 99:677–685

Basu A, Young SW, Suttner LJ et al (1975) Re-evaluation of the use of undulatory extinction and polycrystallinity in detrital quartz for provenance interpretation. J Sediment Res 45:873–882

Beleity A, Ghoneim M, Hinawi M et al (1986) Paleozoic stratigraphy, paleogeography and paleotectonics in the Gulf of Suez. In: 8th EGPC exploration conference, Cairo. pp 17–23

Blatt H (1967) Original characteristics of clastic quartz grains. J Sediment Res 37:401–424

Bowles JFW (2021) Oxides. In: Alderton D, Elias SA (eds) Encyclopedia of geology, 2nd edn. Academic Press, Oxford, pp 428–441

Briden JC (1968) Paleomagnetism of the ntonya ring structure. Malawi. J. Geophys Res 73:725–733

Briden J (1973) Palaeomagnetic Estimate of the Age of the Sebaloka Complex, Sudan, 17th Ann. Rep. Res. In: Inst. Afr. Geol., Univ. Leeds, pp. 33–44

Brock A (1967) Paleomagnetic results from the Hook intrusives, Zambia. Nature 216:359–360

Burke KC, Lytwyn J (1993) Origin of the rift under the Amazon Basin as a result of continental collision during Pan-African time. Int Geol Rev 35:881–897. https://doi.org/10.1080/00206819309465563

Cambeses A, Scarrow JH, Montero P et al (2017) Palaeogeography and crustal evolution of the Ossa-Morena Zone, southwest Iberia, and the North Gondwana margin during the Cambro-Ordovician: a review of isotopic evidence. Int Geol Rev 59:94–130. https://doi.org/10.1080/00206814.2016.1219279

Chima P, Baiyegunhi C, Liu K, Gwavava O (2018) Petrography, modal composition and tectonic provenance of some selected sandstones from the Molteno, Elliot and Clarens Formations, Karoo

Supergroup, in the Eastern Cape Province, South Africa. Open Geosci 10:821–833

Chukhrov FV, Shanin LL, Yermilov LP (1966) Feasibility of absolute-age determination for potassium-carrying manganese minerals. Int Geol Rev 8:278–280. https://doi.org/10.1080/0020681660 9474282

Conoco C (1987) Geological map of Egypt, scale 1: 500,000-NF 36 NE-Bernice, Egypt. Egypt Gen Pet Corp, Cairo

Davies J, Nairn AEM, Ressetar R (1980) The paleomagnetism of certain late Precambrian and early Paleozoic rocks from the Red Sea Hills, Eastern desert, Egypt. J Geophys Res 85:3699–4710

Deer WA, Howie RA, Zussman J (1966) An introduction to the rock-forming minerals, 1st edn. Wiley, Hoboken

Derder MEM, Henry B, Bayou B et al (2006) New African Lower Carboniferous paleomagnetic pole from intrusive rocks of the Tin Serririne basin (Southern border of the Hoggar, Algeria). Tectonophysics 418:89–203

Derder MEM, Henry B, Amenna M, et al (2009) New structural implications for central Sahara (Algeria) from revisited Upper Carboniferous "Hassi Bachir" formation: Paleomagnetic constraints. Tectonophysics 463:69–76

Derder MEM, Henry B, Merabet N, Amenna M, Bourouis S (2001a) Upper Carboniferous paleomagnetic pole from stable Saharan craton and the Gondwana reconstructions. J Afr Earth Sci, 32:491–502

Dickinson WR (1988) Provenance and sediment dispersal in relation to paleotectonics and paleogeography of sedimentary basins BT. In: Kleinspehn KL, Paola C (eds) New perspectives in basin analysis. Springer, New York, pp 3–25

Dickinson WR, Suczek CA (1979) Plate tectonics and sandstone compositions1. Am Assoc Pet Geol Bull 63:2164–2182. https://doi.org/10.1306/2F9188FB-16CE-11D7-8645000102C1865D

Donald RP, Schwab F (1996) An introduction to sedimentary rocks and stratigraphy. W.H. Freeman and Company, New York

Dreher CL, Schad M, Robbins LJ et al (2021) Microbial processes during deposition and diagenesis of Banded Iron Formations. PalZ 95:593–610. https://doi.org/10.1007/s12542-021-00598-z

Eames LE (1984) Palynologic definition of Paleozoic unconformity-bounded sequences, Gulf of Suez region. In: Petroleum exploration and production conf., (EGPC), Cairo. pp 117–125

Ekwenye OC, Nichols G, Mode AW (2015) Journal of African Earth Sciences Sedimentary petrology and provenance interpretation of the sandstone lithofacies of the Paleogene strata, south-eastern Nigeria. J Afr Earth Sci 109:239–262. https://doi.org/10.1016/j.jafrearsci.2015.05.024

El-Barkooky AN (1986) Stratigraphic framework of the Paleozoic in the Gulf of Suez region, Egypt. In: In: First international conference on the geology of the arab world (GAW1), Cairo University, Cairo, Egypt (**abstract**)

El-Bialy MZ, Zoheir BA, Koutsovitis P et al (2023) The anorogenic late Ediacaran granite-rhyolite porphyries of Gabal Abu Durba, Sinai: termination of magmatism in the Neoproterozoic Arabian-Nubian Shield crust. Int Geol Rev 65:843–882. https://doi.org/10.1080/00206814.2022.2079009

Elhebiry MS, Sultan M, Abu El-Leil I et al (2020) Paleozoic glaciation in NE Africa: field and remote sensing-based evidence from the South Eastern Desert of Egypt. Int Geol Rev 62:1187–1204. https://doi.org/10.1080/00206814.2019.1636416

El-Shahat A, Kora M (1986) Petrology of the early Paleozoic rocks of Um Bogma area, Sinai. Mansoura Sci Bull 13:151–184

Eschard R, Abdallah H, Braik F, Desaubliaux G (2005) The Lower Paleozoic succession in the Tasilli outcrops, Algeria: sedimentology and sequence Stratigraphy. First Break 23:27–36. https://doi.org/10.3997/1365-2397.23.1088.26708

Fabre J (1988) Les séries Paléozoïques d'Afrique: une approche. J Afr Earth Sci (and Middle East) 7:1–40

Farahat ES, Zaki R, Hauzenberger C, Sami M (2011) Neoproterozoic calc-alkaline peraluminous granitoids of the Deleihimmi pluton, Central Eastern Desert, Egypt: implications for transition from late- to post-collisional tectonomagmatic evolution in the northern Arabian-Nubian Shield. Geol J 46:544–560. https://doi.org/10.1002/gj.1289

Fernández-Suárez J, Gutiérrez-Alonso G, Pastor-Galán D et al (2014) The Ediacaran-Early Cambrian detrital zircon record of NW Iberia: possible sources and paleogeographic constraints. Int J Earth Sci 103:1335–1357. https://doi.org/10.1007/s00531-013-0923-3

Fisher RA (1953) Dispersion on a sphere. Proc R Soc Lond Ser A Math Phys Sci 217:295–305

Folk RL (1974) Petrology of sedimentary rocks, 2nd edn. Hemphill Press, Austin

Folk RL (1980) Petrology of sedimentary rocks. Hemphill Publishing Co., Austin

Gao Y, Li G, Liu Z et al (2023) Detrital zircon U-Pb isotopes and whole-rock geochemistry of early Palaeozoic sedimentary rocks of the Baoshan and Lancang Blocks, SW China: implications for Proto-Tethys evolution and Gondwana reconstruction. Geol J 58:1870–1891. https://doi.org/10.1002/gj.4697

Ghandour IM, Tawfik HA, Maejima W, Abdel-Hameed AMT (2013) Sedimentary facies and Sequence stratigraphy of the Cambrian Araba formation, Gebel Somr El-Qaa'a, North Wadi Qena, Egypt. Neues Jahrb Fur Geol Und Palaontologie - Abhandlungen 268:149–174. https://doi.org/10.1127/0077-7749/2013/0324

Ghienne J-F, Boumendjel K, Paris F et al (2007a) The Cambrian-Ordovician succession in the Ougarta Range (western Algeria, North Africa) and interference of the Late Ordovician glaciation on the development of Lower Paleozoic transgression on northern Gondwana. Bull Geosci 82:183–214. https://doi.org/10.3140/bull.geosci.2007.03.183

Ghienne JF, Le Heron DP, Moreau J et al (2007b) The Late Ordovician Glacial Sedimentary System of the North Gondwana Platform. Glacial sedimentary processes and products. Wiley, Hoboken, pp 295–319

Gürsu S, Göncüoglu MC (2006) Petrogenesis and tectonic setting of Cadomian felsic igneous rocks, Sandıklı area of the western Taurides, Turkey. Int J Earth Sci 95:741–757. https://doi.org/10.1007/s00531-005-0064-4

Gvirtzman G, Weissbrod T (1984) The Hercynian geanticline of Helez and the Late Palaeozoic history of the Levant. Geol Soc Lond Spec Publ 17:177–186

Haldar SK, Tišljar J (2014) Chapter 2—Basic mineralogy. In: Haldar SK, Tišljar JBT-I to M, P (eds) Elsevier, Oxford, pp 39–79

Hammed MS, Sayed F, Shided AG, Hussein AW (2022) Structural architecture and tectonic evolution of the Shabrawet Syrian Arc inverted zone at the Northern termination of the Gulf of Suez rift, Egypt. Int Geol Rev 64:2941–2965. https://doi.org/10.1080/00206814.2021.2021558

Hanaor DAH, Sorrell CC (2011) Review of the anatase to rutile phase transformation. J Mater Sci 46:855–874. https://doi.org/10.1007/s10853-010-5113-0

Hare JC, Nairn AEM (1990) The Ras'Gharib dikes, Red Sea Hills (Egypt): An uplift origin of the secondary magnetic components. J African Earth Sci 11:55–67

Hassan AA (1967) A new carboniferous occurrence in Abu Durba, Sinai, Egypt (abstract). In: In: 6th Arab petroleum conference, Baghdad, 39 B-3

Hou Q, Mou C, Wang Q, Tan Z (2018) Provenance and tectonic setting of the Early and Middle Devonian Xueshan Formation, the North Qilian Belt, China. Geol J 53:1404–1422. https://doi.org/10.1002/gj.2963

Ibrahim AAE-S (1996) Petroleum geology of the Cretaceous and pre-Cretaceous sedimentary rocks in some oil fields in the Gulf of Suez Area, A. R. Egypt, Ph.D. thesis, Cairo Univ.

Issawi B, Osman R (1996) The sandstone enigma of south Egypt. In: In: 3rd International conference on the geology of the Arab World. Cairo University. pp 359–380

Issawi B, Jux U (1982) Contributions to the stratigraphy of the Paleozoic rocks in Egypt. Geol Surv Egypt 64:28

Jackson M (1990) Diagenetic sources of stable remanence in remagnetized paleozoic cratonic carbonates: a rock magnetic study. J Geophys Res Solid Earth 95:2753–2761. https://doi.org/10.1029/JB095iB03p02753

Khalifa MA, Soliman HE, Wanas HA (2006) The Cambrian Araba Formation in northeastern Egypt: facies and depositional environments. J Asian Earth Sci 27:873–884. https://doi.org/10.1016/j.jseaes.2005.09.003

Khedr ES (2010) the Paleozoic-Mesozoic first order Megasequences in Egypt. Bull Tethys Geol Soc Cairo 5:105–130

Klitzsch E, Gröschke M, Herrmann-Degen W, Said R (1990) Paleozoic and pre-Campanian Cretaceous strata at Wadi Qena. Geology of Egypt. Balkema, Rotterdam, Boston, pp 321–327

Kroner A, McWilliams MO, Germs GJB, Reid AB, Schalk KEL (1980) Paleomagnetism of late precambrian to early paleozoic mixtite bearing formations in Namibia (southwest Africa): the nama group and blaubeker formation. Am J Sci 280:942–968

Kozdrój W, Kennedy AK, Johnson PR et al (2018) Geochronology in the southern Midyan terrane: a review of constraints on the timing of magmatic pulses and tectonic evolution in a northwestern part of the Arabian Shield. Int Geol Rev 60:1290–1319. https://doi.org/10.1080/00206814.2017.1385425

Kruglyakov VV, Kruglyakova GI (1967) Value of epeirogenic curves in interpreting spatial distribution of the geomagnetic field. Int Geol Rev 9:785–792. https://doi.org/10.1080/00206816709474514

Liu H, Chen T, Zou X et al (2013) Thermal treatment of natural goethite: thermal transformation and physical properties. Thermochim Acta 568:115–121. https://doi.org/10.1016/j.tca.2013.06.027

Mange MA, Maurer H (2012) Heavy minerals in colour. Springer Science & Business Media, Berlin

Martin DL, Nairn AEM, Noltimier HC, Petty MH, Schmidt TJ (1978) Paleozoic and Mesozoic paleomagnetic results from Morocco. Tectonophysics 44:91–114

Maurirv JC (1993) The Pan-African West-Congo Belt: links with Eastern Brazil and geodynamical reconstruction. Int Geol Rev 35:436–452. https://doi.org/10.1080/00206819309465538

Maxbauer DP, Feinberg JM, Fox DL (2016) MAX UnMix: a web application for unmixing magnetic coercivity distributions. Comput Geosci 95:140–145. https://doi.org/10.1016/j.cageo.2016.07.009

Meert JG, Van Der Voo R (1997) The assembly of Gondwana 800–550 Ma. J Geodyn 23:223–235. https://doi.org/10.1016/S0264-3707(96)00046-4

Meert JG, Pivarunas AF, Evans DAD et al (2020) The magnificent seven: a proposal for modest revision of the Van der Voo (1990) quality index. Tectonophys 790:228549

Miah AT (2021) Chapter 11—Visible light responsive titania-based nanostructures for photocatalytic reduction of carbon dioxide. In: Nguyen Tri P, Wu H, Nguyen TA et al (eds) Micro and nano technologies. Elsevier, Hoboken, pp 239–266

Mohammad AT, El Kazzaz YA, Hassan SM, Taha MMN (2020) Neoproterozoic tectonic evolution and exhumation history of transpressional shear zones in the East African orogen: implications from kinematic analysis of Meatiq area, Central Eastern Desert of Egypt. Int J Earth Sci 109:253–279. https://doi.org/10.1007/s00531-019-01801-y

Murphy JB, Pisarevsky SA, Nance RD, Keppie JD (2004) Neoproterozoic—Early Paleozoic evolution of peri-Gondwanan terranes: implications for Laurentia-Gondwana connections. Int J Earth Sci 93:659–682. https://doi.org/10.1007/s00531-004-0412-9

Murphy JB, Nance RD, Dostal J, Quesada C (2014) Rifts, arcs and orogens in space and time: a volume in honor of J. Duncan Keppie—an introduction. Int J Earth Sci 103:1181–1186. https://doi.org/10.1007/s00531-014-1028-3

Mvondo H, Betsi TB, McFarlane CRM et al (2023) U-Pb and Ar-Ar geochronological constraints on timing of deformation and peak metamorphism in the Central Africa Orogenic Belt, Yaoundé Domain, Cameroon. Int Geol Rev. https://doi.org/10.1080/00206814.2023.2225183

Nairn AEM, Perry TA, Ressetar R, Rogers SA (1987) Paleomagnetic study of the Dokhan volcanic formation and younger granites, eastern desert of Egypt. J African Earth Sci 6:353–365

Nassr MN (1985) Contrasts between Quartz Grain Shapes of the Cambrian and the Carboniferous 'nubia' Facies in Gabal Abu Durba, Sinai, Egypt, Ph.D. thesis, Univ, South Carolina

O'Brien SJ, Wardle RJ, King AF (1983) The Avalon Zone: a Pan-African terrane in the Appalachian Orogen of Canada. Geol J 18:195–222. https://doi.org/10.1002/gj.3350180302

Omer MF, Friis H, Kokfelt TF, Thomsen TB (2021) Provenance of northern Gondwana Lower Ordovician sandstones (Khabour Formation, northern Iraq) revealed by detrital zircon using LA-ICP-MS dating. Geol J 56:4905–4922. https://doi.org/10.1002/gj.4210

Ouabid M, Garrido CJ, Ouali H et al (2021) Late Cadomian rifting of the NW Gondwana margin and the reworking of Precambrian crust—evidence from bimodal magmatism in the early Paleozoic Moroccan Meseta. Int Geol Rev 63:2013–2036. https://doi.org/10.1080/00206814.2020.1818301

Perrin M, Prévot M (1988) Uncertainties about the Proterozoic and Paleozoic polar wander path of the West African craton and Gondwana: evidence for successive remagnetization events. Earth Sci Lett 88:337–347

Pettijohn FJ, Potter PE, Siever R et al (1972) Petrographic classification and glossary. Sand sandstone. Springer, New York, pp 149–174

Pickerill RK (1983) Lower Palaeozoic of the Middle East, Eastern and Southern Africa, and Antarctica, C. H. Holland (Ed.), Wiley, Chichester, New York, Brisbane, Toronto, 1981. No. of pages: 331. Price: £90.25. Geol J 18:189–190. https://doi.org/10.1002/gj.3350180215

Powell CM, Li ZX, McElhinny MW et al (1993) Paleomagnetic constraints on timing of the Neoproterozoic breakup of Rodinia and the Cambrian formation of Gondwana. Geology 21:889–892. https://doi.org/10.1130/0091-7613(1993)021%3c0889:PCOTOT%3e2.3.CO;2

Razvalyayev AV (1972) Some distinctive aspects of the structure and geologic history of the western Arabia rift system. Int Geol Rev 14:738–747. https://doi.org/10.1080/00206817209475756

Said R (1990) The geology of Egypt. Balkema, Rotterdam

Said SM, Sakran S (2022) Geometry and kinematics of right-lateral transpressional faults and growth folds, the western side of the Gulf of Suez, Egypt. Geol J 57:276–291. https://doi.org/10.1002/gj.4297

Saleh A (2020) Paleomagnetism of Late Neoproterozoic African Dike Swarms from the South Eastern Desert and the Paleo-Neoproterozoic Dataset from Egypt. Pure Appl Geophys 177:5251–5262

Salem AMK, Abdel-Wahab A, McBride EF (1998) Diagenesis of shallowly buried cratonic sandstones, southwest Sinai, Egypt. Sediment Geol 119:311–335

Saradeth S, Soffel H, Horn P, Muller-Sohnius D, Schult A (1989) Upper Proterozoic and Phanerozoic pole positions and Potassium-Argon (K-Ar) ages from the East Sahara craton. Geophys J 97:209–221

Schandelmeier H, Darbyshire DPF, Harms U, Richter A (1988) The East Saharan Craton: evidence for pre-Pan-African crust in NE Africa west of the Nile. In: The Pan-African belt of Northeast Africa and adjacent areas: tectonic evolution and economic aspects of a late proterozoic oregon. Pp pp 69–94

Schütz KI (1994) Structure and Stratigraphy of the Gulf of Suez, Egypt. Inter Rift Basins 59:57–96

Sehsah H, Eldosouky AM (2022) Neoproterozoic hybrid forearc—MOR ophiolite belts in the northern Arabian-Nubian Shield: no evidence for back-arc tectonic setting. Int Geol Rev 64:151–163. https://doi.org/10.1080/00206814.2020.1836523

Seilacher A (1990) The Paleozoic trace fossils. In: Said R (ed) The Geology of Egypt. Balkema, Rotterdam, Brookfield

Semtner A-K, Klitzsch E (1994) Early Paleozoic paleogeography of the northern Gondwana margin: new evidence for Ordovician-Silurian glaciation. Geol Rundschau 83:743–751. https://doi.org/10.1007/BF00251072

Şengör AMC, Lom N, Zabcı C et al (2022) The Saharides: Turkic-type orogeny in Afro-Arabia. Int J Earth Sci 111:2885–2924. https://doi.org/10.1007/s00531-021-02063-3

Soffel, H.C., Saradeth, S., Briden, J.C., Bachtadse, V. and Rolf C (1990) The Sabaloka ring complex revisited: palaeomagnetism and rock magnetism. Geophys J Int, 102:411–420

Soliman SM, Abu El-Fetouh M (1970) Carboniferous of Egypt: isopach and lithofacies maps. Am Assoc Pet Geol Bull 54:1918–1930

Salmon E, Edel JB, Pique A, Westphal M (1988) Carboniferous palaeomagnetic investigations in Morocco: Permian remagnetizations and possible large Carboniferous rotations occurring in Mesetian sedimentary and Jebilets intrusive rocks. Geophys J 93:115–125

Stern RJ (1985) The Najd fault system, Saudi Arabia and Egypt: a late Precambrian rift-related transform system? Tectonics 4:497–511

Tarling DH, Hrouda F (1993) The magnetic anisotropy of rocks. Chapman & Hall, London, p 217

Tawfik HA, Ghandour IM, Maejima W, Abdel-Hameed AMT (2011) Petrography and geochemistry of the lower Paleozoic Araba Formation northern eastern desert Egypt: implications for provenance tectonic setting and weathering signature. J Geosci 54:1–16

Tawfik HA, Ghandour IM, Maejima W et al (2015) Petrography and geochemistry of the siliciclastic Araba Formation (Cambrian), east Sinai, Egypt: implications for provenance, tectonic setting and source weathering. Geol Mag 154:1–23. https://doi.org/10.1017/S0016756815000771

Tawfik HA, Ghandour IM, Salem AM, Maejima W (2012) Petrochemistry of the Lower Cambrian Araba Formation, Taba Area, East Sinai, Egypt. Am Assoc Pet Geol Annu Conv Exhib Long Beach, California, Abstr 50655

Tchameni R, Sun F, Dawaï D et al (2016) Zircon dating and mineralogy of the Mokong Pan-African magmatic epidote-bearing granite (North Cameroon). Int J Earth Sci 105:1811–1830. https://doi.org/10.1007/s00531-015-1276-x

Torsvik TH, Cocks LRM (2004) Earth geography from 400 to 250 Ma: a palaeomagnetic, faunal and facies review. J Geol Soc Lond 161:555–572. https://doi.org/10.1144/0016-764903-098

Torsvik TH, Cocks LRM (2011) The Palaeozoic palaeogeography of central Gondwana. Form. Evol. Africa A Synopsis 3.8 Ga Earth Hist. 357:0

Torsvik TH, Van der Voo R, Preeden U et al (2012) Phanerozoic polar wander, palaeogeography and dynamics. Earth Sci Rev 114:325–368

Toto EA, Kaabouben F, Zouhri L et al (2008) Geological evolution and structural style of the Palaeozoic Tafilalt sub-basin, eastern Anti-Atlas (Morocco, North Africa). Geol J 43:59–73. https://doi.org/10.1002/gj.1098

Van der Voo R (1990) The reliability of paleomagnetic data. Tectonophysics 184:1–9

Wanas HA (2011) The Lower Paleozoic rock units in Egypt: an overview. Geosci Front 2:491–507. https://doi.org/10.1016/j.gsf.2011.06.004

Wanas HA, Soliman HE (2001) Allogenic and authigenic clays of the Lower Palæozoic sandstones of the Naqus Formation at Gebel Gunna, central Sinai, Egypt: their recognition and geological significance. J Afr Earth Sci 32:47–60. https://doi.org/10.1016/S0899-5362(01)90018-1

Wang Y, Hendy IL, Latimer JC, Bilardello D (2019) Diagenesis and iron paleo-redox proxies: new perspectives from magnetic and iron speciation analyses in the Santa Barbara Basin. Chem Geol 519:95–109. https://doi.org/10.1016/j.chemgeo.2019.04.018

Xu C, Rowley DB, Jiayu R et al (1997) Late Precambrian through Early Paleozoic Stratigraphic and Tectonic Evolution of the Nanling Region, Hunan Province, South China. Int Geol Rev 39:469–478. https://doi.org/10.1080/00206819709465285

Zijderveld JDA (1967) AC demagnetization of rocks: Analysis of results. In: Collinson D, Creer K, Runcorn (eds) Methods in palaeomagnetism. Elsevier, Amsterdam, pp 254–286